Sensitivity shift of the meta-metabolome and photosynthesis to the chemical stress in periphyton between months along one year and a half period: Case study of a terbuthylazine exposure

Arthur Medina, Mélissa Eon, Nicolas Mazzella, Chloé Bonnineau, Débora Millan-Navarro, Aurélie Moreira, Soizic Morin, Nicolas Creusot

Science of the Total Environment 957 (2024) 177681

Contents lists available at ScienceDirect

Science of the Total Environment

journal homepage: www.elsevier.com/locate/scitotenv

Sensitivity shift of the meta-metabolome and photosynthesis to the chemical stress in periphyton between months along one year and a half period: Case study of a terbuthylazine exposure

Arthur Medina [a], Melissa Eon [a,b], Nicolas Mazzella [a,b], Chloé Bonnineau [a], Débora Millan-Navarro [a], Aurelie Moreira [a,b], Soizic Morin [a], Nicolas Creusot [a,b,*]

[a] INRAE Nouvelle-Aquitaine Bordeaux, UR EABX, 50 avenue de Verdun, Cestas 33612, France
[b] Plateforme Bordeaux Metabolome, F-33140 Villenave d'Ornon, France

HIGHLIGHTS

- Periphyton meta-metabolome and photosynthesis sensitivity to terbuthylazine was assessed monthly in distinct sampling periods
- Sensitivity benchmark-doses threshold were determined and compared for both biological parameters
- Strong molecular sensitivity shift versus low physiological sensitivity shift were noted
- Contribution of putative metabolites classes differed, suggesting potential different toxicity pathways of the herbicide
- Oxylipins were modulated at all months and correlated with photosynthesis

GRAPHICAL ABSTRACT

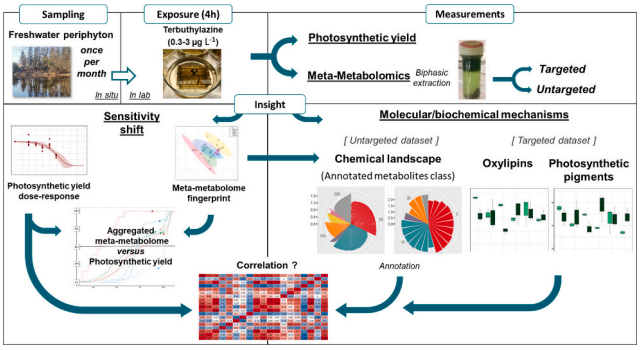

ARTICLE INFO

Editor: Sergi Sabater

Keywords:
Untargeted meta-metabolomics
Microbial ecotoxicology
Sensitivity shift
Herbicide
Annual longitudinal study

ABSTRACT

Despite the knowledge of the effects of contaminants on periphyton, information is limited about their natural fluctuations in sensitivity to chemical stress between various months. In particular, the molecular and biochemical mechanisms associated with sensitivity of photosynthesis and its fluctuations remain poorly described. To tackle this lack of knowledge, meta-metabolomics offers a comprehensive picture of the sensitive molecular response preceding the physiological impact. This study aimed to describe changes in the sensitivity of periphyton to chemical stress at different months over one year and a half period, at both the physiological and molecular levels by measuring photosynthetic yield and meta-metabolome responses (targeted and untargeted approaches). Periphyton was colonized for four weeks and then exposed to a range of terbuthylazine concentrations (0.3–30 µg L^{-1}) under controlled conditions for 4 h. Sensitivity was assessed by determining the benchmark doses for the meta-metabolome and photosynthesis, along with the cumulative distribution of aggregated metabolomics signals. The results showed a strong sensitivity shift in the meta-metabolome compared to a smaller shift in photosynthetic yield at different months. This study also confirmed the high sensitivity of the meta-metabolome, as most signals responded before photosynthesis. The annotation highlighted the discrepancies in the molecular response to TBA between the months in terms of metabolite classes (e.g. amino acids,

* Corresponding author.
E-mail address: nicolas.creusot@inrae.fr (N. Creusot).

https://doi.org/10.1016/j.scitotenv.2024.177681
Received 30 June 2024; Received in revised form 17 November 2024; Accepted 19 November 2024
Available online 23 November 2024

alkaloids, and lipids), their sensitivity, and trends in common classes across months, and correlation to photosynthesis inhibition, notably oxylipins. Overall, this study highlights that the molecular response of the periphyton to chemical stress, and thus toxicity pathways, may differ between the months but can still lead to similar physiological responses.

1. Introduction

Agriculture contributes to aquatic chemical pollution by releasing xenobiotics, especially organic herbicides. These chemicals are suspected to affect non-target aquatic organisms in addition to the target species (Beketov et al., 2013; Schreiner et al., 2016; Vonk and Kraak, 2020). For instance, certain herbicides can impair the photosynthetic activity of microbial primary producers, potentially risking ecological functions and services. Photosynthesis is an essential physiological function that ensures the growth of phototrophs and sustainability of the food web (Bonnineau et al., 2020).

Microbial communities are increasingly used in ecotoxicological studies to enhance ecological impact assessment and evaluate such potential ecological impairment (Pesce et al., 2018; Guasch et al., 2016; Tlili et al., 2010). Freshwater microbial periphytic communities (periphyton) are ubiquitous complex assemblages of microorganisms that settle on inorganic substrates (e.g. rocks). They are composed of eukaryotic (e.g. microalgae, fungi, and protozoa) and prokaryotic (e.g. bacteria, viruses, and cyanobacteria) microorganisms (Watnick and Kolter, 2000). These organisms exert various nutritional strategies (*i.e.* autotrophy, heterotrophy, and mixotrophy) and provide different key ecosystem functions (*i.e.* biogeochemical cycles, overall detoxification, and biomass production) in aquatic ecosystems (Morin and Artigas, 2023; Bonnineau et al., 2020; Beronius et al., 2020; Battin et al., 2016). Diatoms, cyanobacteria, and green algae dominate the autotrophic periphyton composition and support the food web as major primary producers directly associated with their photosynthetic activities, ensuring the growth and production of energy-rich molecules (Gomes and Juneau, 2017; Herlory, 2005).

Clear evidence exists regarding the ability of several organic herbicides to impair the metabolism, cell growth, and photosynthetic activity of freshwater periphyton (Smedbol et al., 2018; Chaumet et al., 2020; Tlili et al., 2008). For example, the herbicide triazine family (photosystem II (PSII) inhibitor) can impair PSII electron flux by binding to serine in the *Hill* reaction complex (D1 protein) and inducing an increase in oxidative species due to the accumulation of harvested and untransformed light energy. Oxidative stress accumulation induces the peroxidation of different compounds, such as lipids and pigments (Asada, 2006; Battaglino et al., 2021; Wang et al., 2022). Proia et al. (2013) also reported an inhibitory effect from triazine herbicides (*i.e.* atrazine, simazine, terbuthylazine) at environmental concentrations on photosynthetic yield and photo-pigments (chlorophyll *a* density, μg cm^{-2}). Even though photosynthetic activity measurements (*e.g.* photosynthetic yield) are relevant descriptors for assessing the potential impairment of photosynthetic function in phototrophic biofilms, knowledge about the natural fluctuation on its sensitivity to chemical stress lacks. This limits the interpretation of these descriptors, and that is also a general statement for multiple other descriptors (*e.g.* antioxidant and extracellular enzymatic activities) (Sabater et al., 2016). In particular, the underlying molecular and biochemical mechanisms associated with the alteration of photosynthetic function at the community level and involved in the fluctuation of its sensitivity remain unclear (Creusot et al., 2022).

Omics enables the direct assessment of molecular responses at the community level to elucidate such mechanisms. The use of liquid chromatography-high-resolution mass spectrometry (LC/HRMS-MS)-based untargeted metabolomics is particularly relevant because it can simultaneously assess the internal chemical exposome and the associated molecular phenotype (endometabolome) (Creusot et al., 2022; Gauthier et al., 2020). Several studies have demonstrated that metabolites can be used as early and sensitive descriptors of response to toxicants in various organisms (Delignette-Muller et al., 2023; Bedia, 2022; Li et al., 2018). As such, metabolomics applied to microbial communities (i.e. meta-metabolomics) combined with other microbial descriptors (i.e. photosynthesis, structure, and function) at the community level would fill the knowledge gap regarding the relationship between exposure and potential impairment of community homeostasis (Colas et al., 2023; Creusot et al., 2022; Gil Solsona et al., 2021). However, elucidating such mechanisms can be challenging because current metabolite databases enable only the annotation of a small portion of the detected metabolites (Dias et al., 2016). Recent studies have partly addressed this issue by annotating metabolites at the class level (ClassyFire, Natural Compounds Classifier ontologies), which enables preliminary assumptions about the modulated biochemical pathways (Kim et al., 2021; Djoumbou Feunang et al., 2016). Moreover, there is evidence for the relevance of aggregated omics responses in providing a comprehensive picture of the molecular/biochemical response to chemical stress (Larras et al., 2018, 2020). These approaches further support the prioritisation of the signals for their annotation or classification as potential defence vs damage responses according to their trends (*i.e.* mono/biphasic) and threshold level responses (*i.e.* the benchmark dose) (Colas et al., 2023; EFSA Scientific Committee, 2017; Creusot et al., 2022).

In this context, the aims of this study were to describe the variation in the meta-metabolome and photosynthesis sensitivity of periphyton collected at different months and exposed to a model herbicide, and further highlight the metabolites classes related to these responses, especially those potentially involved in the photosynthesis modulation by this herbicide. According to the literature, it was hypothesized that periphyton sensitivity to chemical pressure would fluctuate between different months because of changes in environmental parameters and community composition variation (Tien et al., 2013). In addition, the meta-metabolome response was expected to be more sensitive to terbuthylazine exposure than photosynthesis, as it happens at the molecular level. This characterisation would further help to better understand the relationship between the meta-metabolome and the photosynthetic response to chemical stress and further obtain biochemical insights into the impairment of photosynthesis.

In particular, PSII inhibition could potentially lead to changes in pigment concentration, such as chlorophyll *a* and carotenoid content within the photosystem. Periphytic communities were sampled monthly during one year and a half and exposed for 4 h to a concentration range of the model herbicide terbuthylazine (TBA) (Cañero et al., 2011). Following exposure, meta-metabolome and photosynthesis sensitivities were assessed through untargeted/targeted metabolomics and photosynthetic yield measurements and compared through the determination of benchmark dose responses. In particular, an untargeted approach was implemented to obtain a comprehensive picture of the meta-metabolome response and provide insight about the metabolites classes involved in the effects of TBA on periphyton. Additionally, targeted analyses were performed to identify the photosynthetic pigments and lipids that respond to TBA exposure to induce oxidative stress because TBA targets PSII plastoquinone B.

2. Materials and methods

Owing to the sheer amount of data and information, supporting information is provided in the form of a Word document containing additional details and supplementary Figures and Excel sheets

containing additional data. These are referred to as "SI manuscript" and "SI tabular", respectively, throughout the main manuscript.

2.1. Chemicals, reagents, and stock solution

Terbuthylazine (CAS N°5915-41-3) was purchased at Dr. Ehrenstorfer (purity: 98.69 %, France) and prepared in acetonitrile (ACN, ULC/MS grade, Biosolve, France) to obtain a stock solution of 8 g L^{-1} stored at −20 °C. The extraction solvents used were ultrapure water (UPW), methyl-tert-butyl ether, and methanol (ULC/MS grade, Biosolve). ultra-high-performance liquid chromatography (UHPLC) grade eluents were prepared using ACN, water (ULC/MS grade), isopropanol (ULC/MS grade), formic acid (FA, purity: 99 %), and ammonium formate (AF, powder, purity: 99 %), all purchased from Biosolve.

Mixtures of analytical grade standards (1 mg L^{-1} concentration) used for targeted analysis were: i) mixtures of phytoplankton pigments (PPS-MIX-1 127, HPLC grade, DHI group) and ii) oxylipins standard 9(*S*)-HOTrE (9S-hydroxy-10E,12Z,15Z-octadecatrienoic acid, Cayman chem, France; CAS: 89886-42-0, purity >98 %), 9-HODE ((±)-9-hydroxy-10E,12Z-octadecadienoic acid (Cayman chem, France; CAS: 98524-19-7, purity>98 %) and 12(*S*)-HETE (12S-hydroxy-5Z,8Z,10E,14Z-ecosatetraenoic acid, Cayman chem, France; CAS: 54397-83-0, purity >95 %).

2.2. Field sampling and laboratory exposure

In the present study, periphyton was sampled for eight months over a period of 12 months from April 2022 to April 2023. Owing to extreme weather events, the pound was dry from September to November 2022 and sampling in August (2023) was repeated. Each month, glass slides (L: 76 mm- l: 26 mm) were colonized by periphyton for four weeks in the hypereutrophic Gazinet-Cestas pond (South West France, geographical coordinates 44°46′30.1″N, 0°41′44.3″W, Fig. S1) (Neury-Ormanni, 2021). Following the sampling, periphyton was acclimatised for 16 h in an indoor aquarium filled with filtrated pond water (45 μm) under controlled temperature (set temperature = colonization period mean temperature) and light (LED JBL SOLAR NATUR, 200+ μM S^{-1} m^{-2}, 6300 lm, daylight white spectrum) using a 12 h alternated photoperiod (light phase 8 A.M–8 P.M). The incident light intensity on the slides was measured using a light meter (LI-COR Li-250, USA). Meteorological conditions for April 2022 and April 2023 are provided in SI Tabular Sheet 1. In addition, the algal group composition (cyanobacteria, green algae, diatoms) in the pound periphyton was estimated based on chlorophyll fluorescence at specific wavelengths (green 470 nm, blue 645 nm, brown 470 nm, and 520 nm) (Schmitt-Jansen and Altenburger, 2005), using PhytoPAM instrument (see Section 2.3 for details). Data are provided in SI Tabular Sheet 1.

The periphyton was then exposed to a serial dilution of terbuthylazine (TBA) (0, 0.3, 1, 3, 10, 30 μg L^{-1}) in 500 mL glass beakers (five replicates per concentration) for 4 h under the same conditions. The TBA concentration range was selected according to the scientific literature to encompass both environmentally relevant concentrations and algal EC_{50}s (Finizio et al., 2022; Vonk and Kraak, 2020; Proia et al., 2013). TBA was resuspended in ACN and the exposure volume was 300 mL with a final ACN concentration of 0.05 % under all conditions. The experimental conditions (herbicide concentration gradient, periphyton suspension volume, exposure period, and ACN concentration) were optimised prior to the study to ensure measurement comparability (data not shown). In particular 0.05 % of ACN was defined in accordance with previous experiments in our laboratory (Chaumet et al. and Ornany et al., unpublished data; Creusot et al., 2022), the ACN control concentration used for meta-metabolome and photosynthesis was below the 0.25 % concentration where no effect was observed on periphyton. For safety, and due to the absence of a water control, the ACN concentration was set five times lower than the no observed effect concentration. The exposure solution was transferred to each beaker for equilibration for 2 h before randomly adding six glass slides to each beaker for 4 h. Following exposure, one glass slide was collected from each beaker for the measurement of photosynthetic activity (see Section 2.3), while the five others were pooled and used for metabolomics analyses (see Section 2.4). The sampling measurement methodology and analytical strategy are summarised as a workflow in Fig. S2.

2.3. Measurement and data analysis of the photosynthetic activity

Inhibition of photosynthetic activity by TBA was assessed by measuring the photosynthetic yield, which determines the physiological state of autotrophic organisms (Chaumet et al., 2020; Morin et al., 2018). This was performed using a PHYTO-PAM fluorimeter (Pulse-Amplitude Modulated) (Heinz Walz, GmbH, Germany) equipped with an emitter-detector unit (PHYTO-ED). This instrument quantifies the relationship between the photosystem photonic energy conversion efficiency and chlorophyll fluorescence quenching (Corcoll et al., 2012). Periphyton was scraped from one glass slide (39.52 cm^2) using a toothbrush and suspended in 9 mL of their respective exposure water (4.39 cm^2 mL^{-1}) immediately after sampling. Then, 3 mL of suspension of each sample replicate per exposure condition was added to 1 cm wide 3 mL quartz cuvettes, and photosynthetic yield was assessed during a saturating light pulse after 3 min of light adaptation; five measurements remained (15–20 s between each saturating pulse).

Data acquired from the PHYTO-PAM were processed and analysed using R studio software (v4.2.3, Posit software PBC, 2023).

Firstly, a statistical comparison of yield measurement between the concentrations (control vs exposed) for each month were performed using non-parametric univariate *Kruskal–Wallis* tests (p-value ≤0.05 accepting alternate hypothesis). Tests were coupled with *Dunn* post hoc test adjustment (p-adjust = 0.05), false discovery rate test (FDR, *Benjamin–Hochberg* test summarised in SI Tabular Sheet 2). The test was selected based on effective size and the non-fulfilment of normal data distribution for some months (visual confirmation by density plot and QQ plot, *Shapiro* test p-value > 0.05).

Secondly, dose-response curve models were adjusted for the photosynthetic yield response of samples exposed to a gradient of TBA to obtain toxicity threshold values for each month. The photosynthetic yield–dose responses to the TBA curves were modelled after log-2 transformation of the data using the DRomics 2.5-0 tool (Shiny version, https://lbbe.univ-lyon1.fr/fr/dromics, Larras et al., 2018). The model's benchmark dose (BMD_{1SD}) was determined, enabling further comparison with the meta-metabolome response. Quadratic dose responses were fitted to the experimental data according to five models of regression (linear, exponential, *Hill*, *Gauss-probit*, and log-*Gauss-probit*) and classified as monophasic (increase or decrease) or biphasic (bell and U-shape) (see SI manuscript Section 1.3.1). BMD_{1SD} values were then determined using the formula 'BMR-zSD = y0 ± z*SD', where y0 is the mean control response, SD is the residual standard deviation of the considered concentration-response model, and z is the factor of SD (z fixed at 1 by default) (EFSA Scientific Committee et al., 2009, 2017). Next, BMD_{1SD} confidence interval (CI) (confidence threshold set at 0.99) was calculated using non-parametric approach on model residuals, using an ANOVA-like test with 10,000 iterations and p-value acceptance set at $p < 0.01$ (see SI Tabular Sheet 3). Bootstrap CI and the number of iterations were chosen based on the number of replicates per condition (n = 4 or 5) and a recent recommendation for parametric estimator determination. BMD_{1SD} is a statistically significant toxicity threshold, which indicates that the lowest concentration induces a significant change compared to the control (*i.e.* solvent control). In addition, the method used to calculate the CI makes it a reliable and robust discriminatory indicator (>0.005 % error rate) (Larras et al., 2018). Significant differences in photosynthetic sensitivity between months were determined by comparing the CIs of $BMD_{1SD,}$ with non-overlapping CIs indicating significant differences between BMD_{1SD}.

2.4. Untargeted and targeted meta-metabolomics

2.4.1. Quenching and sample preparation

Following 4 h of exposure, five glass slides from each of the five replicate beakers were wrapped in aluminium foil and immediately quenched in liquid nitrogen (−196 °C) and stored at −80 °C prior to freeze drying and further extraction.

Freeze drying was performed for 24–48 h with a gravimetric control. Then, periphyton was scrapped from the five glass slides for each replicate with a razor blade, pooled in aluminium foil, and stored at −80 °C prior the extraction. Metabolites were extracted according to the liquid/solid and liquid/liquid biphasic methods described by Mazzella et al. (2023). Briefly, a mean of 9.2 mg (± 0.1 SE) of dried biomass was added to 2 mL microtubes containing 150 mg microbeads (0.5 mm diameter). Extraction was performed by the sequential use of a mixture of (1) methyl-tert-butyl-ether and methanol (MTBE-MeOH, ratio 3:1, v:v) and ultrapure water and methanol (UPW-MeOH, ratio 3:1, v:v), which enabled the separation and further collection of hydrophilic metabolites (aqueous phase) and lipophilic metabolites (MTBE phase) (see SI manuscript Section 1.4.1). Following the extraction, 500 μL of each phase were dried independently using a rotary evaporator (Speed-VAC SPD121P, Thermo Fisher) at 30 °C and 1 mbar for 1 h using aqueous vs organic mode until a few drops remained before resuspension in 100 μL of UPLC grade H_2O-ACN (50:50, v:v) for the hydrophilic fraction and in 100 μL of UPLC grade ACN-Isopropanol (50:50, v:v) for the lipophilic fraction. Both fractions were centrifuged prior to injection (5 min at 3500 rpm) to pellet the particles and avoid blocking the UPLC system.

2.4.2. UPLC-HRMS/MS analyses

Untargeted and targeted meta-metabolomics analyses were performed on hydrophilic and lipophilic fractions, respectively. This was performed using UHPLC combined with a time-of-flight (TOF) HRMS system (UHPLC-HClass-Xevo G2-S ToF, Waters) as described by Tison-Rosebery et al. (2023). Briefly, 10 μL of each fraction (hydrophilic and lipophilic) were injected and separated on a reverse-phase ACQUITY HSST3 RP-C18 column (150 × 2.1 mm × 1.7 μM, Waters) as reported in the SI manuscript (Section 1.4.2). The samples were ionised for both untargeted and targeted analyses using an electrospray ionisation (ESI) source operated in the positive (POS) and negative (NEG) modes with MSE acquisition, according to the parameters detailed in Table S4. Quality control for the UPLC-TOF analyses is described in the SI manuscript (Section 1.4.3). A mixture of analytical standards of oxilipins and photosynthetic pigments was injected at 1 mg L^{-1} concentration prior to the samples for targeted analysis of the lipophilic fraction to determine the retention time and fragmentation pattern.

Further analyses were performed on a UHPLC Vanquish coupled to a Q-Exactive Plus mass spectrometer equipped with a heated electrospray ionisation (HESI-II) probe (Q-Exative+, Thermo Fisher Scientific, San Jose, CA) to obtain more accurate MS/MS spectra because of the low match of the TOF–MSE spectrum with MS/MS databases (*e.g.* MONA, MASS-BANK, and HMDB). Thus, the hydrophilic fraction samples were analysed using parallel reaction monitoring (PRM) acquisition to focus the annotation on the most relevant features from the chemometric analysis of the TOF data (see Sections 2.4.3 and 2.4.4). An inclusion list of 100 features was defined for each month and polarity (see Section 2.4.4). Each list was further divided into 50 features to improve PRM acquisition with closely related compounds (*m/z* and Rt). The chromatographic conditions were the same as those used for the TOF system to maximise the matching of the mass spectrometry dataset. The QEx + acquisition parameters in POS and NEG modes are listed in Table S5.

2.4.3. Data processing

The data processing pipeline is illustrated in Fig. 1. All software parameters are described in detail in the SI manuscript (Sections 1.4.4–1.4.10). The POS and NEG untargeted metabolomics datasets were processed into two distinct datasets for every month. They were subjected to the same parameters in different analytical steps until annotation and subsequent aggregation.

Briefly, untargeted metabolomics data from the hydrophilic fraction analysis on UPLC-TOF were processed in Workflow4Metabolomics

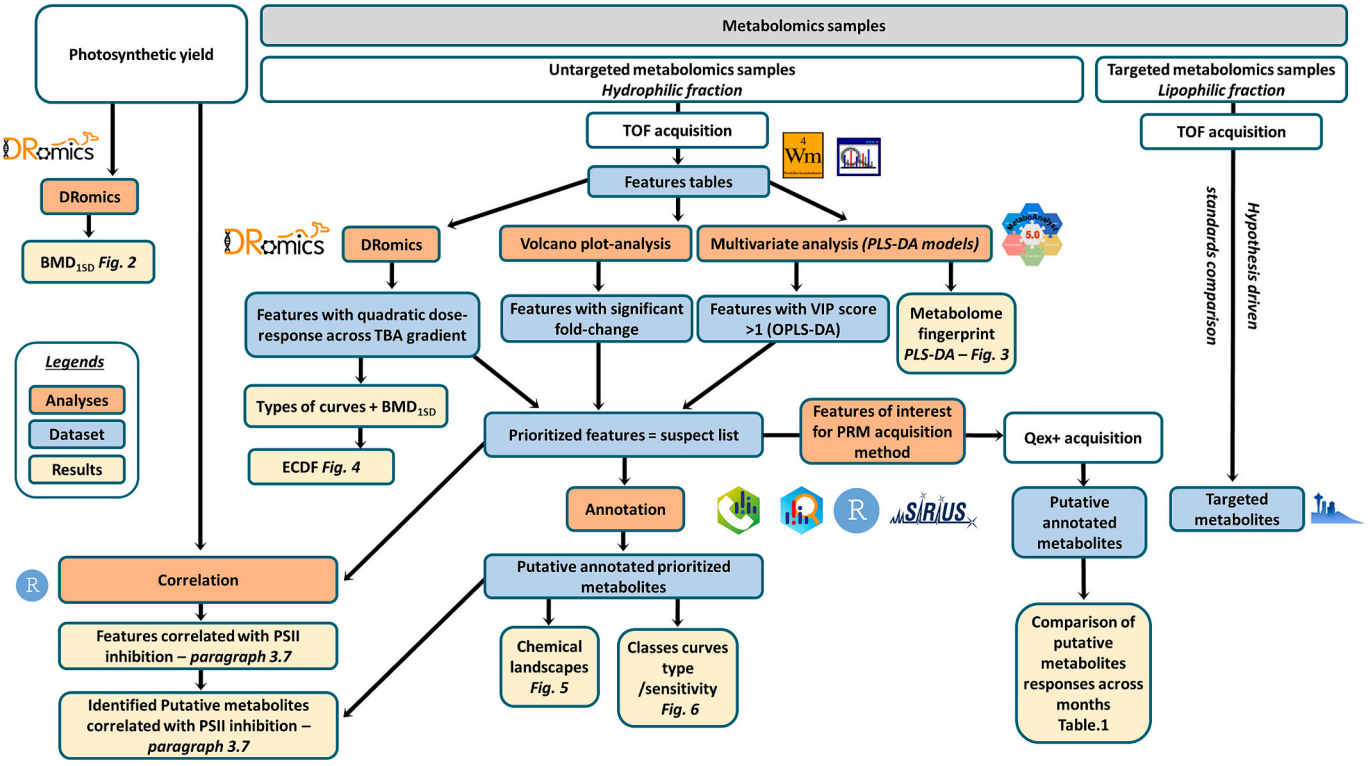

Fig. 1. Data analysis pipeline.

(W4M, Giacomoni et al., 2014) as previously described by Creusot et al. (2022). The parameters of preprocessing and further filtration are summarised in Section 1.4.4. Owing to the large amount of data, which was higher than that permitted on the Galaxy, each month was processed independently. Feature intensities were normalised to their respective dry weights to ensure comparability of the detected signals (number and intensity).

Data from the UPLC-QEx analysis of the hydrophilic groups were processed following the methodology described by Tison-Rosebery et al. (2023). Briefly, raw data were processed using MS-Dial (v4.9.3, Tsugawa et al., 2015) and annotated using the MS-Finder (v3.60, Tsugawa et al., 2016) and SIRIUS 5 (Dührkop et al., 2019) tools. Methodologies are detailed below in 2.4.5 and software parameters are summarised in SI manuscript Sections 1.4.7–1.4.10.

2.4.4. Chemometrics pipeline for hydrophilic untargeted dataset

The TOF feature lists were first analysed using MetaboAnalyst (v5.0, https://www.metaboanalyst.ca/; Xia et al., 2009). Interquartile range (IQR) filtration was performed for lists with >5000 features prior to data analysis. All datasets then underwent sample median normalisation, data cube root transformation, and data Pareto scaling, in accordance with Nyamundanda et al. (2010). Partial least squares discriminant analysis (PLS-DA) was performed on all datasets to evaluate general tendencies in and between sample group conditions (*e.g.* dose-response tendency).

The transformed data were analysed using the DRomics R package to assess the whole dose response (v2.5.0, Larras et al., 2018). For each metabolomic signal, a trend (increase, decrease, U-shape, bell) and a unique BMD_{1SD} were determined by fitting with quadratic regression, following Larras et al. (2018) (SI manuscript Section 1.3.5). Overall metabolome fluctuations and sensitivity to nominal contaminant concentrations were summarised using an empirical cumulative distribution function (ECDF) representation and previously selected signals. These ECDF distributions and their BMD_{1SD} CIs (bootstrap sampling number set at 1000 with 0.95 confidence interval) were statistically compared. This comparison was performed using a linear model for each ECDF (formula = log10 (BMD) − months). The least squares mean of the linear model was used to predict the marginal mean of each month to estimate the linear combinations of the model parameters. Then using pairwise test and Tukey adjustment ($\alpha = 0.05$), the marginal mean and the standard error computed were statistically compared (see SI Tabular Sheet 4).

The two most discriminated samples (control vs highest concentration) were compared to highlight the responses of the metabolomics signals that did not present a quadratic dose-response trend. Firstly, univariate analysis-based volcano plots were used to identify significant differences in feature intensity (fold-change threshold = 2, Wilcoxon Rank test, $p < 0.05$, with FDR correction). Multivariate orthogonal PLS-DA (OPLS-DA) was then performed to identify the signals that contributed the most to the discrimination between the two conditions (*i.e.* variable of importance (VIP)).

Finally, the most relevant features prioritised by each data analysis encompassing DROMICS (signals following a quadratic trend with a BMD_{1SD} value), OPLS-DA (signals with a VIP score > 1), and volcano plot analysis (significant signals, fold >1.25, $p < 0.05$ FDR) were grouped into suspect lists (*i.e.* one per polarity for each month) (Fig. 1 and SI Tabular Sheet 5).

2.4.5. Feature and metabolite classes annotation

Annotation of the features and their classes was performed by combining the MS-DIAL (v4.9.2; Tsugawa et al., 2015), MS-CleanR (R package v1.0, Fraisier-Vannier et al., 2020), MS-Finder (v3.6.0; Tsugawa et al., 2015), and SIRIUS 5 (v5.8.3; Dührkop et al., 2019) software packages, as described by Tison-Rosebery et al. (2023). Data processing and software settings are detailed in SI manuscript Sections 1.3.6–1.3.9. Overall, MS-FINDER and SIRIUS 5 enabled the investigation of several structural and spectral databases (PubChem, KEGG, HMDB, and COCONUT) based on the MS2 spectra. In particular, CANOPUS (Kim et al., 2021) in SIRIUS 5 provided a means to classify features according to the ClassyFire and Natural Compounds Classifier ontologies (Kim et al., 2021; Djoumbou Feunang et al., 2016). Due to low matches between our MS2 spectra and existing databases or predicted spectra or fingerprints and overall low-level confidence, annotation was performed at the metabolite class level using NPC ontology (SI Tabular Sheet 6). The specific number of annotated metabolite classes is summarised in SI Tabular Sheet 5, whereas the global proportion and the percentages of each class per month are summarised in SI Tabular Sheet 7.

Following annotation, the chemical landscapes of the TOF dataset (aggregated hydrophilic fractions, POS and NEG) were represented for each month using a circular histogram (R package ggplot2 v3.4.3) based on the VIP score (common to all filtered data). In addition, using a DRomics interpreter (Delignette-Muller et al., 2023; Larras et al., 2020, see SI manuscript Section 2.3 for details), annotated TOF datasets were plotted as cumulative sensitivity and trends.

An additional acquisition was performed using a UPLC-Qex + instrument to enhance the confidence level of structural identification (see SI manuscript, Section 1.3.2). Qex + data were processed as described in SI manuscript, Sections 1.3.6–1.3.9. Putatively annotated compounds were categorised in Levels 2b and 3 confidence ratings based on the Schymanski et al. (2014) guidelines (MS2 library spectrum or in silico predicted MS2 match) and summarised in SI Tabular Sheet 8.

2.4.6. Targeted metabolomics data processing and statistics

Targeted metabolomics datasets from lipophilic fraction analyses were processed using Skyline software (v23.1, https://skyline.ms/, Henderson et al., 2018; MacLean et al., 2010). The software parameters are detailed in SI manuscript Section 1.3.4. The main peak intensity and area under the curve were exported for further analysis. Statistical comparisons were performed between the exposure conditions specific for each month (April 2022 and April 2023) using non-parametric tests due to non-compliance with normality (visual confirmation and *Shapiro-Wilk* test) and a low number of replicates ($n < 30$). Non-parametric univariate *Kruskal–Wallis* tests (p-value ≤0.05 accepting alternate hypothesis) with *Dunn* post hoc test correction (p-adjust ≤0.05) were performed to statistically differentiate metabolite intensity between TBA exposure at each month (SI Tabular Sheet 9).

2.5. Meta-metabolomics vs photosynthetic yield datasets

Firstly, the sensitivities of the metabolome and photosynthesis to TBA were compared using the photosynthetic yield BMD_{1SD} as a threshold value to interpret the whole metabolome sensitivity distribution. Then, in the suspect list, annotated compounds common to different months were compared and discriminate by their individual BMD_{1SD} and CI values. In addition, *Kruskal–Wallis* tests followed by *Dunn's* post hoc tests (p-value ≤0.05, p- adjust <0.05, FDR test) were performed, as described in Section 2.3, to compare the months for each common putative metabolite (see SI Tabular Sheet 10).

A correlation matrix was determined using the Pearson correlation coefficient and all acquired metabolomics (targeted and untargeted) data (stats package R v4.2.3, cor() function, Becker et al., 1988) to highlight the putative metabolite classes and annotated and unannotated metabolites potentially involved in the photosynthetic yield response. Metabolite correlation values >0.45 or < −0.45 threshold were kept based on Toubiana and Maruenda (2021) guidelines and prioritised metabolite results (see SI Tabular Sheet 11).

Linear modelling (single and multiple) was performed to strengthen the correlation between the common prioritised metabolites and the photosynthetic response (p-value <0.05, F-value > F-critical value, dot distribution between [−2,2], SI Tabular Sheet 12).

2.6. Quality assurance and quality control

Prior to exposure, glass beakers, iron racks and glass slides were flushed with water and ethanol, then heated to 450 °C for 8 h to eliminate residual contamination.

The effective exposure concentrations were measured using UPLC-TOF HRMS. TBA concentrations were calculated based on external calibration by using peak area value and compared to a standard concentration range of TBA from 1 μg L^{-1} to 0.3 mg L^{-1}. The results are presented in SI Tabular Sheet 13 and show similar concentrations between months.

The coefficient of variation (CV) of the number of signals per month was calculated (standard deviation/mean) on an untargeted metabolomics dataset at each analytical step to assess the variability and consistency of the data along the analytical pipeline between months (Lee et al., 2019). The aim of this indicator was to identify the loss of information between the different datasets processed and analysed individually.

3. Results

3.1. Photosynthetic yield response

TBA significantly inhibited the photosynthetic yield of periphyton following 4 h of the highest concentration (see SI Tabular Sheet 2 for pairwise test results of the control vs other conditions). The intensity of inhibition, expressed as a proportion of the control condition, ranged from approximately 42 to 72 % of that of the control response. BMD_{1SD} was determined from dose-response quadratic modelling (Fig. S3) and plotted in Fig. 2 to highlight changes in the sensitivity of photosynthetic yield throughout the year.

BMD_{1SD} values results fluctuated from 0.55 ± [0.12; 3.17] for the most sensitive communities in April 2023, to 10.61 ± [4.73; 22.8] μg L^{-1} for less sensitive communities in August 2023. Three groups of microbial sensitivity to TBA were identified. The first group comprised communities sampled in April 2022, July 2022 and August 2023 (Group a, ± [4.73; 22.8] μg L^{-1}) with low sensitivity. The second group comprised communities sampled in August 2022 and April 2023 (Group b, ± [0.12; 4.5] μg L^{-1}) with higher sensitivity. Finally, the BMD_{1SD} of the microbial communities sampled on the other months were not statistically different from these two groups as shown by CI overlapping (Group ab, ± [0.64; 12.02] μg L^{-1}) (SI Tabular Sheet 3). This shift in photosynthetic yield sensitivity contrasts with the changes in periphyton algal composition observed between April 2022 and August 2023 (SI Tabular Sheet 1).

3.2. Signal dispersion along untargeted metabolomics pipeline

As there was a discrepancy in the number of signals per month of the period between the ionisation modes and, in general, along the analytical pipeline, the CVs were calculated based on the number of signals per month for each analytical approach. The CV was determined as a quantitative indicator to measure the variability between months during data analysis. The CV computed in SI Tabular Sheet 5 was separated by polarity until aggregation. The CV value of the untargeted dataset fluctuated between the different analytical steps, *i.e.* from 0.37 (POS) and 0.61 (NEG) up to 1.2 after DRomics statistical analysis. With the aggregation of both the POS and NEG datasets, the CV decreased to 0.89 post-annotation.

After data processing, 2332 to 9289 signals were detected in positive mode (POS) and 382 to 13046 signals in negative mode (NEG). Following manual data correction, the initial number of signals ranged from 1599 to 5441 in POS and from 354 to 9055 in NEG, depending on the month. The number of signals in the statistically prioritised dataset for annotation ranged from 82 to 1567 between the months across the period (representing 2 to 18 % of the original data, POS and NEG combined).

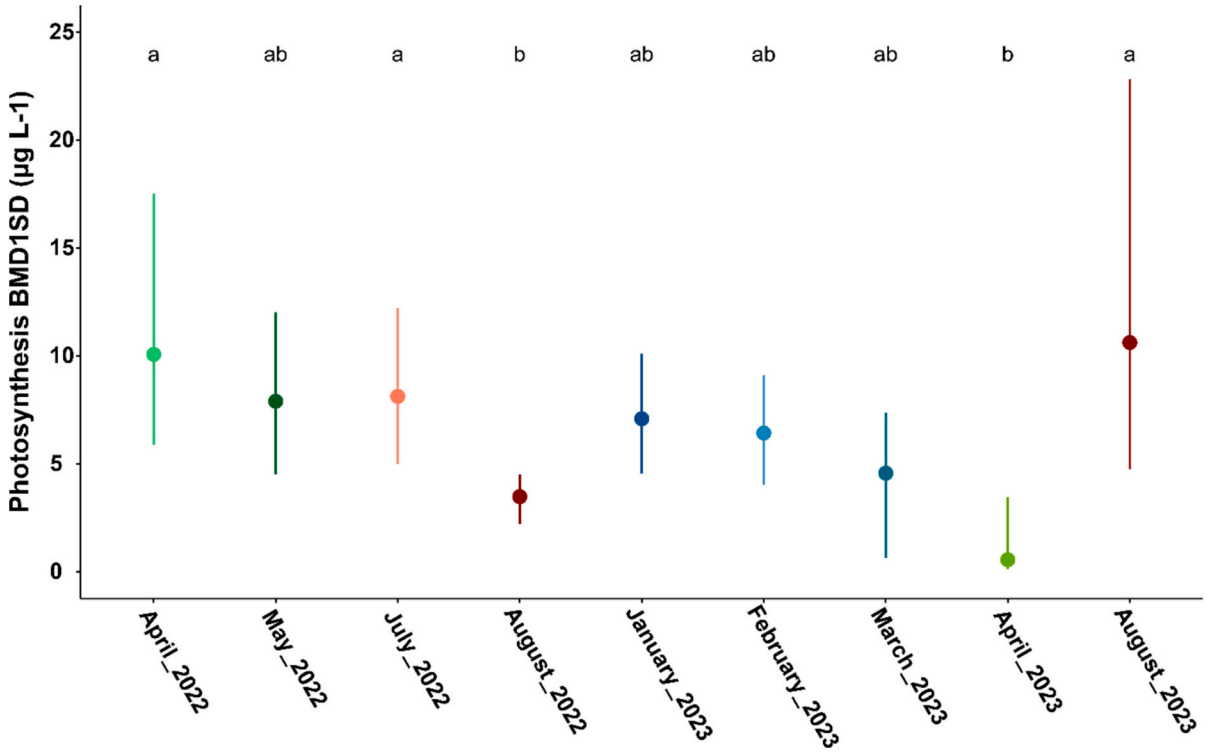

Fig. 2. BMD_{1SD} value of the photosynthetic yield following terbuthylazine exposure. Results are represented as dot plot with upper and lower CI values (99 % confidence score). Non-overlapping CI are considered statistically different. A summary of values and their statistical determinations are provided in SI Tabular Sheet 3.

3.3. Meta-metabolome aggregated response

At first, PLS-DA was performed for each month for both the POS and NEG TOF untargeted datasets (hydrophilic fraction). For the sake of readability, the PLS-DA score plots for April 2022 and February 2023 are presented in Fig. 3, whereas those for the other months are presented in Fig. S4.

PLS-DA revealed that the metabolomics fingerprints differed between the control and exposure conditions for all months. Discrimination underlined the difference between the control and all concentrations, with the highest concentration being the most separated. The exposure conditions were mainly distributed along the first and second axes in a dose-response-like gradient. Here, the first component axis explained between 13.2 and 23.3 % of the total covariance (POS and NEG aggregated) associated with the chemical stress, with a minimum of 9.7 up to 65.2 % reported in Fig. S4. The PLS-DA showed a proper degree of fitting to the data for all months ($R^2 \geq$ 0.64 in POS, $\geq$ 0.74 in NEG). However, the relevance of the focal predictor in some cases ($Q^2 >$ and < 0.4) was not homogeneous, indicating model overfitting.

ECDF was plotted for each dataset to further investigate the dose-dependent responses of the entire meta-metabolome (Fig. 4). The ECDF classification by trend is presented in Figs. S6 and S7.

Firstly, the number of signals identified using DRomics that contributed to each month's ECDF (*i.e.* following a quadratic regression model, FDR <0.05, see SI Tabular Sheet 5) varied from 14 to 997 (POS) and 1 to 611 (NEG) (Fig. 4). Secondly, the representation included only metabolites that responded significantly to the concentration gradient and exhibited a quadratic trend. Depending on the month, this remained between 0.02 % and 27.4 % for the processed dataset. Thirdly, data from April 2023 were excluded from the representation (Fig. 4), because the entire distribution was a single line with a BMD_{1SD} value of 7.07 μg L^{-1}.

The entire metabolomics response for the POS dataset fluctuated significantly between months. For instance, 50 % of the BMD_{1SD} distribution (black horizontal line) were reached before 0.3 μg L^{-1} in May 2022 and August 2022 whereas this threshold was around 10 μg L^{-1} in February 2023 and April 2023 (Fig. 4A). Similarly, seven of the nine months showed that 50–75 % of the whole metabolome response occurred below 2 μg L^{-1} of TBA exposure with the NEG dataset (Fig. 4B). Further statistical analysis revealed that the distributions were significantly different from one month to another ($p < 0.005$) for both POS and NEG datasets (see SI Tabular Sheet 4).

Additionally, almost all the aggregated meta-metabolome ECDF responses (Fig. 4) and metabolite dose-response trends (Figs. S6 and S7)

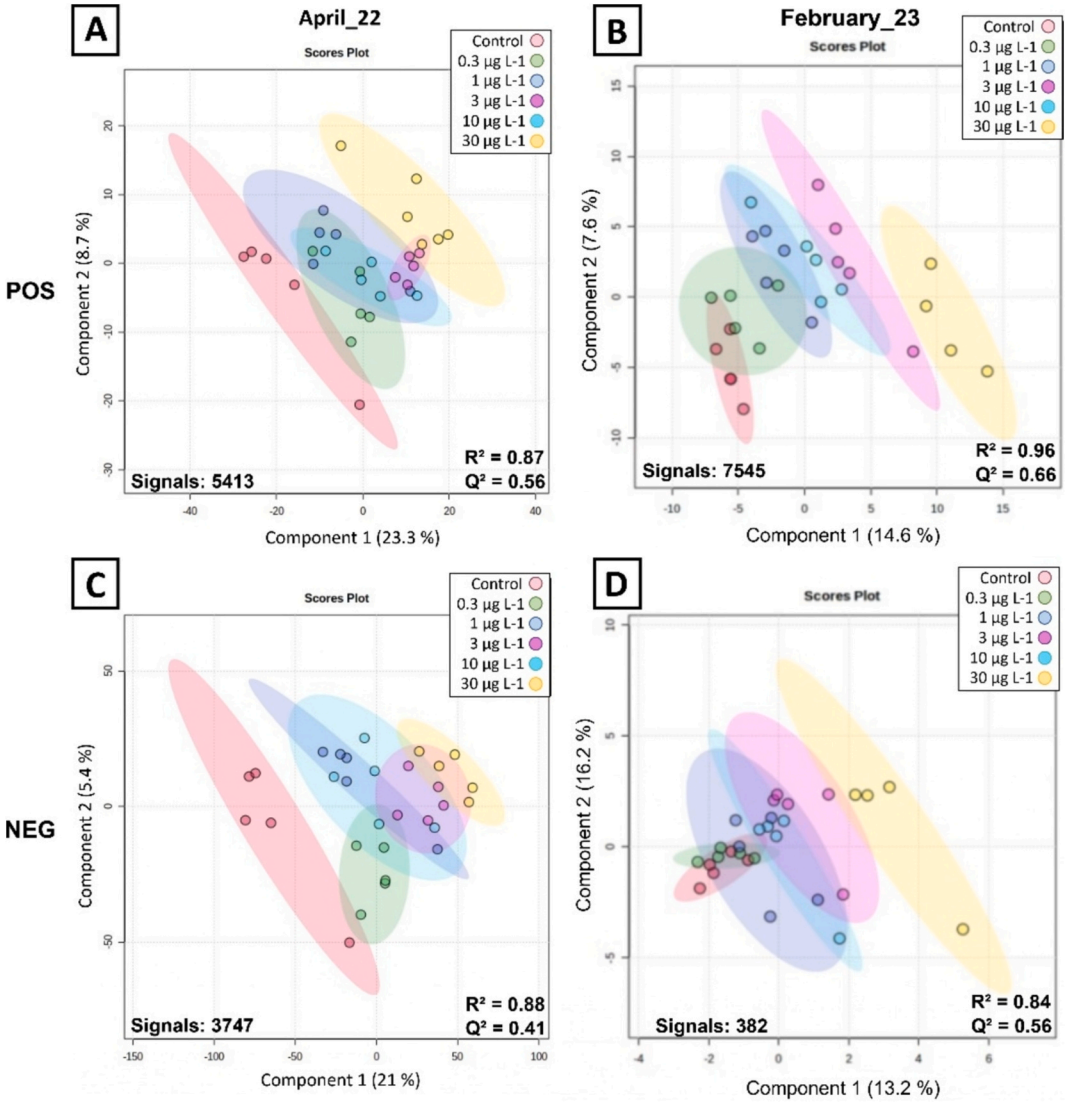

Fig. 3. Score plot of PLS-DA on untargeted meta-metabolomics dataset from April 2022 (**A**, POS, **C**, NEG) and February 2023 (**B**, POS; **D**, NEG). R^2 and Q^2 at the bottom represent the modelling quality indicators. Signals at bottom left indicate the initial number of data used for the PLS modelling.

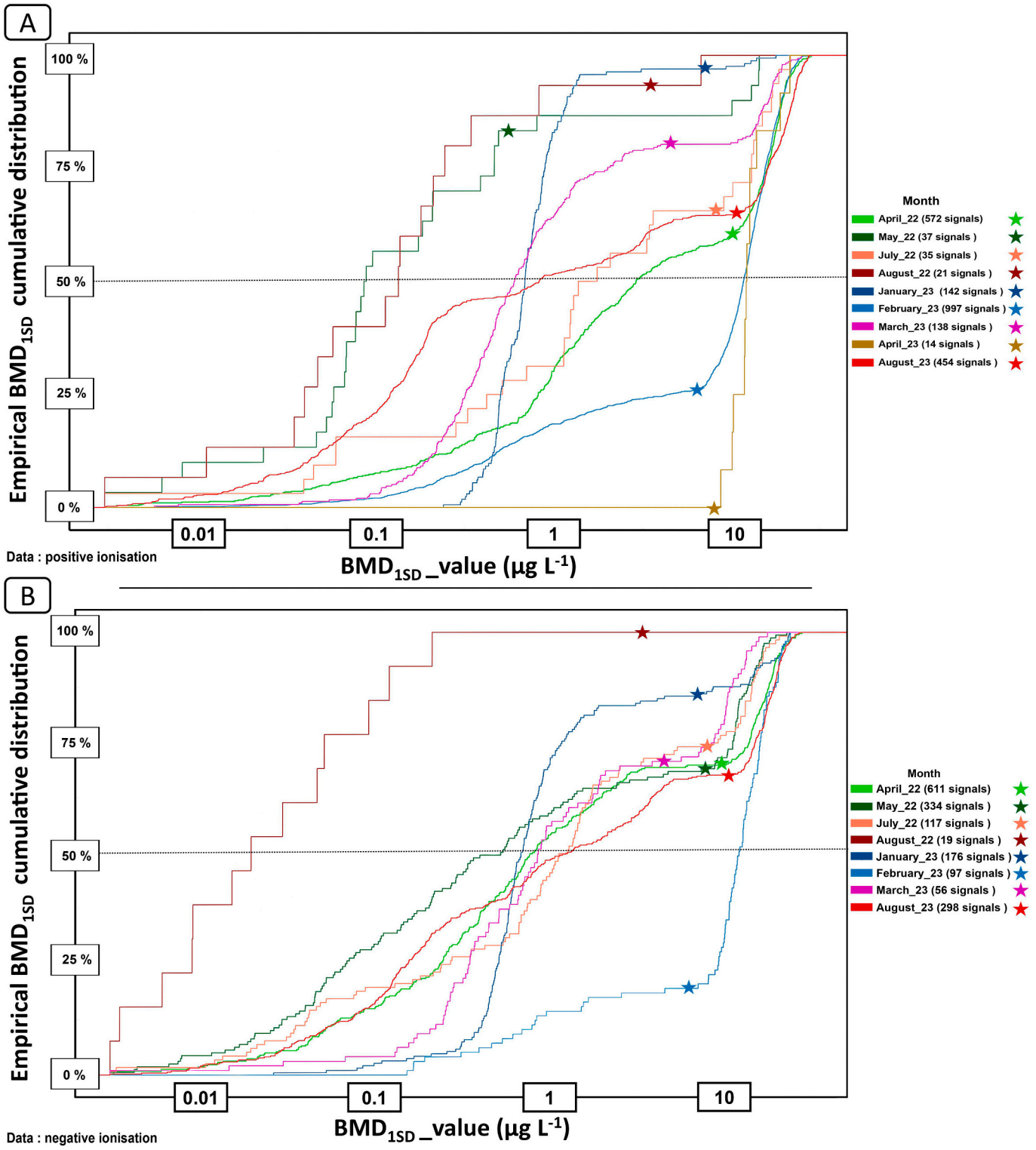

Fig. 4. ECDF of the meta-metabolomics response at each month for POS untargeted dataset **(A)** and NEG untargeted dataset **(B)** along the BMD_{1SD} value (x-axis, LOG in µg L^{-1}). For each month, the star indicates photosynthetic yield BMD_{1SD}. Each individual signal dose-response curve used for the ECDF is detailed in the supplementary information "BMDdrcfit" and separated by month. April_2023 was represented by a single BMD_{1SD} value of 7.07 µg L^{-1}. And as such no represented in the NEG ECDF.

showed three major distribution phase responses: (I) between 0.1 and 1 µg L^{-1}, the ECDF shows a steep slope indicating that an increasing number of metabolites reached BMD_{1SD} in this concentration range; (II) between 3 and 8 µg L^{-1}, the ECDF slope is less steep, indicating that fewer metabolites are reaching their BMD_{1SD} value in this concentration range; (III) over 8 µg L^{-1}, the ECDF slope gets steeper (similarly to Phase I) illustrating an increase in the number of metabolites reaching their BMD_{1SD} value in this concentration range. Moreover, the highest differences between the ECDF trends of the different months (with at least 10 signals) were observed in the concentration range of 0.1–3 µg L^{-1}.

Within these phases (I, II, and III), the trends associated with the BMD_{1SD} values (increase, decrease, U-shaped curve (U), and bell-shaped curve (bell)) differed between months (Fig. S5 and S6). Nevertheless, a majority of months in both polarities had between 50 and 75 % of bell shape curves and 70–100 % of U signals (biphasic trend) BMD_{1SD} in the 0.1–1 μg L^{-1} range of Phase I. Signals with decreasing trends (monophasic trend) had heterogeneous distribution between months; however, all displayed graphical discontinuing distribution in Phase II. Furthermore, except for May 2022 POS and March 2023, between 50 and 80 % of the signals with increasing monotonic trends were in Phase III.

Further comparison of the meta-metabolome BMD_{1SD} cumulative distribution with BMD_{1SD} of the photosynthetic yield (depicted as stars in Fig. 4) revealed that ≥50 % of the metabolome already reacted before the photosynthetic BMD_{1SD} threshold was reached for seven of the nine months in POS (Fig. 4A). Similarly, for NEG (Fig. 4B) dataset, except in February 2023, all months had 60 % or more of the metabolome already reacting before the photosynthetic BMD_{1SD} threshold (Fig. 4B).

3.4. Chemical landscape of the metabolites modulated by the TBA

Overall, MS-Finder and SIRIUS 5 enabled only partial annotation of the TOF datasets in both POS and NEG, with low confidence levels for structural identification. Features with good confidence scores (*i.e.* MS-finder Structure_score > 3, SIRIUS 5 COSMIC confidence score > 0.7) represented <1 % of all the metabolites annotated. Thus, annotation was considered at the metabolite class level according to the NPC (NPC pathway probability >0.5). Therefore, between 1.8 (August 2022) and 81.7 % (July 2022) of signals in the suspect lists were annotated along the different datasets (between 17 and 216 signals). The chemical landscapes of the prioritised significant features for each month are shown in Fig. 5.

Chemical landscapes highlighted that the most represented classes within the putatively annotated metabolites discriminating microbial communities between control and exposed to TBA were alkaloids (37.7 % ± 0.7, $n = 9$) and amino acids and peptides (35.7 % ± 1.3, $n = 9$) for all months (Fig. 4). When present, terpenoids and lipids represented 10.3 % (± 0.4, $n = 8$) and 8.7 % (± 0.5, $n = 8$) of the metabolites while carbohydrates were up to 10 % of the total landscape but absent in August 2022 and 2023 (percentage classes per month in SI Tabular Sheet 7). Nevertheless, the contribution of each class varied between months in terms of the VIP score and the number of features per class in the chemical stress response. Based on the VIP score, alkaloids, amino acids, and peptides were the most important classes for discriminating biofilms exposed to TBA from controls. However, less represented metabolite classes (≤ 6 %), like polyketides in August 2023 or carbohydrates in July 2022, still expressed high scores in their own landscape (top 15).

3.5. Sensitivity and trend response of responsive metabolite classes

The putatively annotated metabolite classes presented in the chemical landscapes, followed by a quadratic trend in dose responses, are presented in Fig. 6.

As depicted in Fig. 6A, the types of quadratic trends (decreasing, increasing, bell, or U-shaped) along the TBA gradient followed by putative metabolites were highly variable across months and different classes. No clear patterns were observed throughout the year. Nevertheless, the number of trends per class and across classes was homogenous in the months with the highest number of metabolites. In the ECDF depicted by month and trend (Fig. S7), putative metabolites with

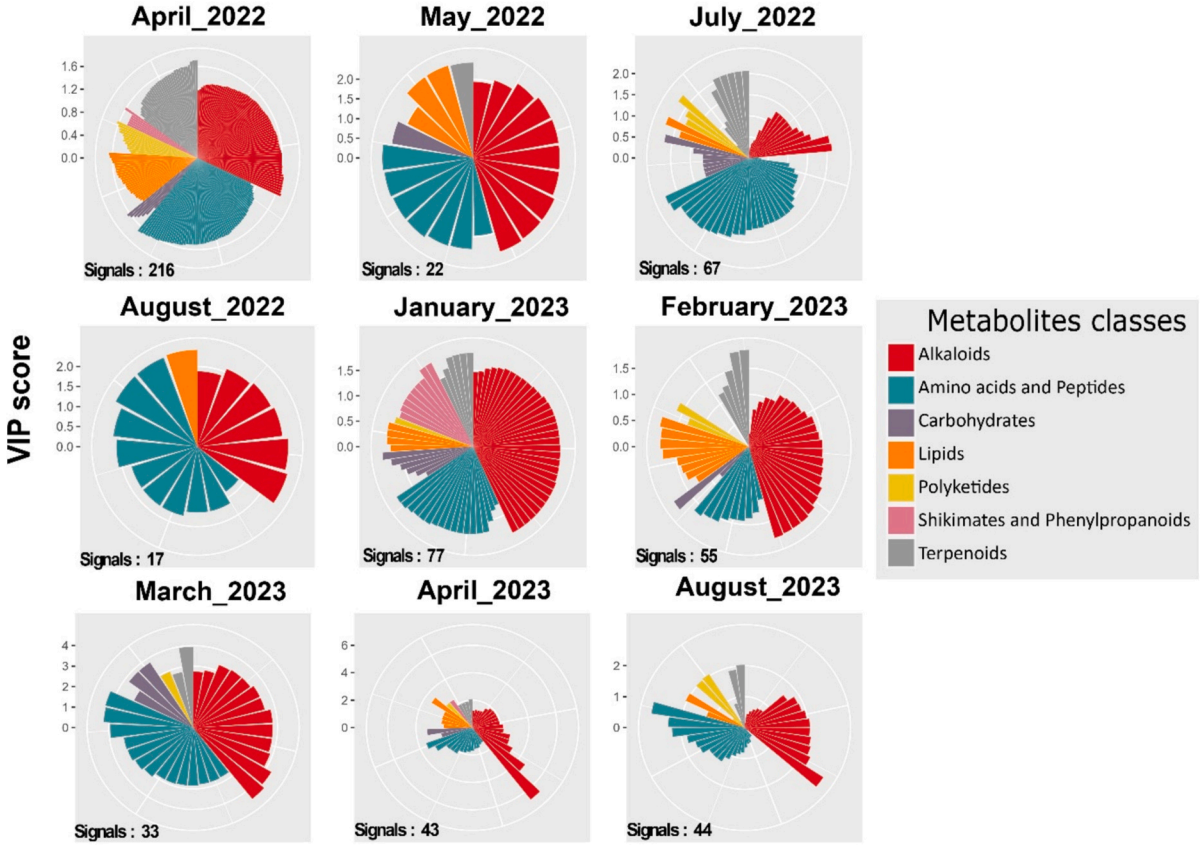

Fig. 5. Chemical landscape depicted as distribution of discriminating (VIP score > 1 between control communities and communities exposed to TBA) responsive putatively annotated (NPC_pathway) metabolite chemical classes per month with TOF untargeted acquired data, POS and NEG dataset are aggregated (annotation detail in SI Tabular Sheet 6). The numbers on the bottom left represent the significant metabolomics signals from the OPLS-DA analysis depicted in the circular diagram for each month.

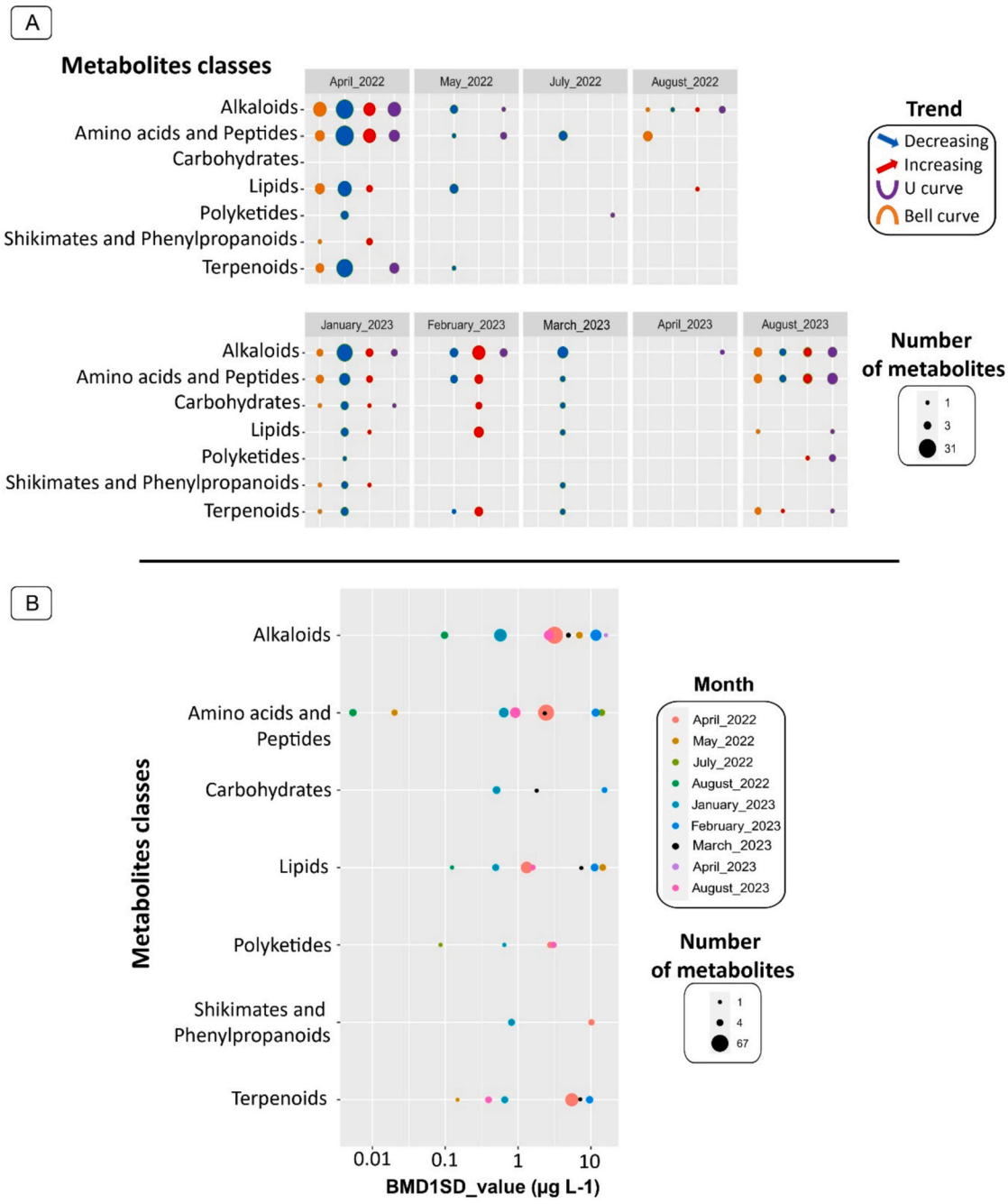

Fig. 6. **(A)** Trend response of metabolite classes for each month. Illustration obtained by combining NPC_pathway annotation (TOF untargeted acquired data, POS and NEG) and corresponding putative metabolite DRomics dose-response modelling dataset in DRomics interpreter shiny application (Delignette-Muller et al., 2023). The size of the dot represents the number of quadratic signals along TBA gradient. **(B)** Sensitivity plot to TBA exposure distribution along the BMD_{1SD} values (x-axis, in µg L^{-1}) of the different metabolite classes (y-axis) per month. Representation obtained by combining NPC_pathway annotation (TOF untargeted acquired data, POS, and NEG) and mean BMD_{1SD} value in DRomics interpreter shiny application. The size of the dot represents the number of quadratic signals along TBA gradient.

biphasic responses (U, bell) were more sensitive to TBA (low BMD_{1SD}) than putative metabolites with monotonic responses (Decreasing, Increasing), with a few exceptions. These results were consistent with the observations of the entire metabolome phases described in Fig. 4. Following the aggregated responses of all the months BMD_{1SD} values, those associated with the biphasic trend distributed mostly below 2 µg L^{-1} (82.5 %). In contrast, those with a monophasic trend were mostly higher than this concentration (64.3 %).

The sensitivity plot (Fig. 6B) reported the distribution of BMD_{1SD} values by metabolite class for each month. It highlights, in the same way as Fig. 6A, that the shift in class sensitivity was more month-specific than a clear response pattern to TBA. Thus, the sensitivity plot underlined that for all classes, the mean BMD_{1SD} were < 1 µg L^{-1} in January 2023 and > 8 µg L^{-1} for February 2023. The metabolites most sensitive to TBA were found within amino acids and peptides with BMD_{1SD} ranging from <0.01 to >10 µg L^{-1}. The second most sensitive metabolites were found within the alkaloids, lipids, polyketides, and terpenoids with BMD_{1SD} ranging from ~0.1 to >10 µg L^{-1}. The metabolites less sensitive were found within the carbohydrates, shikimates and phenylpropanoids with BMD1SD ranging from 0.8 to >10 µg L^{-1}.

Pools of samples (one per month) were injected into a UPLC-Qex + system with an inclusion list corresponding to the prioritised signals

from the TOF datasets to improve the annotation confidence level (see Section 2.4.4). Among putatively annotated metabolites, a few matched the metabolite MS2 spectrum in silico MS/MS (*i.e.* 13-HOTE, Laurenol, Cyclizidine G, N(6)-(Octanoyl)lysine, and Fusapyrone) (L3 annotated level) (SI Tabular Sheet 8). In addition, slight overlap was observed in annotated metabolites (Qex + data) between months. Indeed, only eight metabolites with quadratic dose responses were found over several months (*i.e.* April 2022, May 2022, or February 2023) (Table 1).

Among the eight annotated metabolites, five were lipids (octadecadienoic acid, lactones, and carotenoids), two were alkaloids (macrolides and nitrosopiperidine), and one was a terpenoid (sesquiterpenoid). Except for salinixanthin, all the other compounds exhibited a decreasing trend in response to TBA. Comparison of annotated metabolites sensitivity based the BMD_{1SD} values (CI value, 95 % confidence) and pairwise comparison of the dose response (*Kruskal–Wallis–Dunn* tests, *p*-value ≤ 0.05 and *p*-adjust ≤ 0.05, SI Tabular Sheet 10) showed significant variation for certain months (Table 1).

3.6. Target analyses of lipophilic fraction

According to our hypothesis on oxidative stress induced by TBA, targeted metabolomics analysis was performed on the lipophilic fraction, focusing on photosynthetic pigments (*i.e.* chlorophyll, carotenoid, xanthophyll, and chlorophyllide), glycerol-phospholipids, and oxylipins (*i.e.* HODE, HETE, and HOTrE) in the samples collected in April 2022 and April 2023. These samples were selected because their photosynthetic results differentiated them into two groups separated by a one-year period (see SI Tabular Sheet 1 for weather conditions). Both significant (*i.e.* PG (16.0_18.1), HETE, and HOTrE) and non-significant responses (chlorophyll *a*, chlorophyll *c*2, chlorophyll *b*, pheophorbide *a*, fucoxanthin, zeaxanthin, and lutein) of the targeted metabolites are presented in Fig. S8. Despite the high variability in the response, all significant differences between the control and the highest concentration presented a *p*-value <0.02.

Among targeted lipids, only identified PG (16.0_18.1) showed a significant increase (*Kruskal–Wallis* tests, *p*-value <0.05) in April 2022 (Fig. S8), and among all the targeted oxylipins, only 12-HETE and 9-HOTrE showed a significant inhibition of 71 to 77 % for the month of April 2022 at the highest TBA concentration compared to the control (Fig. S8).

3.7. Correlation between photosynthesis and meta-metabolome responses

Pearson correlation analyses were performed each month between the dose responses of the photosynthetic yield and prioritised features to link the meta-metabolome to the photosynthetic yield responses (*i.e.* from DRomics, volcano plot, and PLS-DA analyses). Between 1.4 (March 2023) and 52.1 % (January 2023) of the prioritised signals were correlated with the photosynthetic response (listed in SI Tabular Sheet 11). Most of the correlated features (80–100 %) were not annotated for all months (August 2022, February 2023, March 2023, and April 2023). May 2022 had slightly more annotated compounds, representing 33.5 % of the correlated signals. Among all annotated metabolites, 77 metabolites were filtered based on their fold-change score, with a maximum correlation score of 0.77 and a minimum of −0.47. Among the putative metabolites, 10 hydroxy fatty acids were prioritised, with a correlation value matching the correlation cutoff (≥ 0.45 or ≤ -0.45). The correlation factor changed between the months for these metabolites. For instance, 9(*S*)-HPODE had a correlation value of 0.65 in February 2023 and − 0.15 in April 2022, and only 9(10)-EpODE had a correlation value of over 0.45 in both months.

Linear and multiple linear regressions were performed to provide further information concerning the link between the meta-metabolome and photosynthetic response (linear model, *p*-value <0.05, SI Tabular Sheet 12). Correlated and uncorrelated putatively annotated metabolites following quadratic dose-response curves are depicted in Fig. S9, S10 and S11 and summarised in the SI Tabular Sheet 8. By adding all common metabolites per month, linear prediction provided a better positive correlation with the photosynthetic response, confirming the previous correlation results. However, the regression presented a goodness of fit (R^2) below 0.5, indicating a low fit between the model and the data.

Uncorrelated features represented between 47.9 % (January 2023) and 98.6 % (March 2023) of the prioritised metabolomics responses. Among these features, most were unannotated (72.4–99.9 %, list in SI Tabular Sheet 5) for all months. For the annotated uncorrelated signals, 69 signals were filtered based on their fold-change scores, with all metabolite classes represented (list in SI Tabular Sheet 11).

4. Discussion

This study investigated the molecular and physiological responses of freshwater periphyton to 4 h TBA exposure following collection in different months during the period at the same location. Our results showed (i) a strong shift in meta-metabolome sensitivity and a lower one in photosynthesis sensitivity to acute TBA exposure, with the meta-metabolome being more sensitive than photosynthesis at all studied time points. The study further highlighted (ii) discrepancies in the

Table 1
Comparison of annotated putative metabolites (from Qex + concatenated datasets) sensitivity and trend response to TBA. Statistical significance according to Kruskal–Wallis–Dunn test over putative metabolite dose-response (see SI Tabular Sheet 10) [ns: > 0.05; *: < 0.05; **: < 0.01; ***: < 0.001]. Note that for the curves trend, dec: decrease and inc: increase.

Compound	Class (sub-class)	Month	*p* value	Trend	BMD_{1sd} (µg L^{-1})	BMD_{1sd} CI	
						Lower	Upper
15(16)-EpODE	Lipids	April 2022	0.014	Dec	15.46	8.76	27.92
		May 2022		Dec	0.032	0.014	0.08
Salinixanthin	Lipids	April 2022	0.049	Inc	0.4	0.01	3.94
		February 2023		Inc	11.23	6.72	17.79
9(10)-EpODE	Lipids	April 2022	0.015	Dec	15.58	8.19	24.80
		May 2022		Dec	0.039	0.015	0.087
9(*S*)-HPODE	Lipids	April 2022	0.35	Dec	14.05	8.15	26.22
		February 2023		Dec	11.04	6.35	18.97
Brefeldin A	Lipids	April 2022	0.5	Dec	3.37	0.691	20.88
		February 2023		Dec	13.9	8.65	24.21
Pernetic acid A methyl ester	Terpenoids	April 2022	0.009	Dec	14.3	8.06	27.18
		May 2022		Dec	0.082	0.038	0.156
2,6-Dimethyl-1-nitrosopiperidine	Alkaloids	April 2022	0.01	Dec	0.191	0.082	0.397
		May 2022		Dec	9.77	5.40	15.33
Zeranol	Alkaloids	April 2022	0.3	Dec	2.84	0.68	17.21
		February 2023		Dec	8.13	4.38	12.63

contribution of putative metabolite classes (*e.g.* signal count, trend, and sensitivity) between the periphytons. Q-Exative-based annotation supported these findings as (iii) few of the more responsive identified metabolites were common across the months of the time frame. Additionally, many unknown metabolites contributed to the overall biochemical responses to TBA. Similarly, (iv) despite a few common classes (*e.g.* oxylipins), most metabolite classes correlated with photosynthesis inhibition differed between months. Each of these major findings is discussed in the following sections.

4.1. Shift of sensitivity to TBA between months at the physiological vs the molecular level

Our results underlined the inhibition of photosynthetic yield under TBA exposure, with significant but minor differences between months during the period. Overall, the sensitivity range (BMD_{1SD} value of 0.6–10.5 μg L-1) was in accordance with previously reported values for microbial communities exposed to TBA or by-products (Battaglino et al., 2021; Margoum et al., 2023; Polst et al., 2023). As this range is of environmental relevance (Tasca et al., 2018), these results question the actual adverse effects of TBA on periphyton photosynthetic activity in natural ecosystems with potentially associated structural and functional impairments. This is of particular concern regarding the key role of these communities in ecosystems in primary production and biogeochemical cycles (Morin and Artigas, 2023; Lips et al., 2022; Bonnineau et al., 2020).

Whole meta-metabolomes showed strong and significant sensitivity shifts throughout the study period. To our knowledge, this study is the first to inform about such shift between several months. This aligns with previous studies indicating that the periphyton meta-metabolome exhibits a time-varying and complex response to herbicides (Lips et al., 2022; Gil Solsona et al., 2021; Rodríguez-Mozaz et al., 2020). For instance, Creusot et al. (2022) demonstrated the variability in the meta-metabolome response during a month-long exposure to diuron. Overall, in line with previous studies, our results showed that the periphyton meta-metabolome response to TBA exposure involves diverse dose-response trends (Colas et al., 2024; Creusot et al., 2022). Furthermore, our results highlighted the specific BMD_{1SD} distribution across the TBA gradient for each dose-response trend, identifying the sensitivity ranges of TBA concentrations for each trend type. These variations in meta-metabolome sensitivity may reflect different types of biological processes (defence versus damage), as suggested by Colas et al. (2023). An initial TBA concentration range, likely corresponding to the defence and acclimatisation mechanisms, was identified at an environmental concentration (<2 μg L^{-1}). In this range, sensitive features mostly followed 'biphasic trend' curves. The second sensitivity range aligns with photosynthetic yield BMD_{1SD} values, with metabolites of this range mainly showing 'monophasic trend' curves, possibly representing damage to the photosystem.

Comparing the two sensitivity responses, meta-metabolome demonstrated greater sensitivity to TBA than to photosynthesis, with half of the meta-metabolome responding at a concentration lower than the photosynthetic yield BMD_{1SD} for nearly all months of the period. This was particularly evident within the environmental concentration range (0.094–1.795 μg L^{-1}) reported in the literature (Eymery et al., 2021; Tasca et al., 2018; Schreiner et al., 2016). At these concentrations, photosynthetic sensitivity differed significantly from the control only in April 2023 and August 2022. Conversely, the meta-metabolome either entered or completed Phase I of its global response for most months. This higher sensitivity aligns with existing literature, confirming the relevance of omics, especially metabolomics, in providing a more sensitive assessment of the whole community response compared to usual descriptors (Colas et al., 2023; Creusot et al., 2022; Serra-Compte et al., 2018).

Altogether, these results showed how the colonization month can modulate measured responses, thereby underlying its importance in biomonitoring. This further questions the outcomes of the cutting-edge omics-based descriptors, especially the metabolomics, compared to traditional descriptors (*e.g.* photosynthesis) in terms of toxicity threshold and actual consequences on the ecosystem functions following acute versus chronic exposure.

4.2. Discrepancies in the meta-metabolome response to TBA between the months

While the whole metabolome signals followed all four trends types (increasing, decreasing, U curve, and bell curve), the putatively annotated metabolite classes were prevalent in only one or two trends, depending on the month (except August 2023). This highlights a loss of information when using only the annotated dataset. Despite this limitation, the chemical landscape still depicted a contrasting picture of the meta-metabolome's response to TBA. On the one hand, it revealed that only alkaloids, lipids, amino acids, and peptides were consistently modulated by TBA throughout the year. On the other hand, the number of signals within these classes, as well as their trends and sensitivity, differed for the months of the surveyed period.

Although these discrepancies (number of signals, sensitivity, trends among metabolites classes) between the months were not clearly elucidated in the present study, they may have various origins. It is likely that the basal meta-metabolome changes over the years because it is highly sensitive to environmental changes. For example, Creusot et al. (2022) showed that temperature, light, and river flow modulate the periphyton meta-metabolome. Similarly, Rožman et al. (2023) reported that intermittent flow alters microbial community metabolome, particularly affecting dissolved organic matter-related microbial activities (*e.g.* production, degradation). Changes in the basal metabolome may affect microbial sensitivity through trade-offs in energy resource allocation (Garrido et al., 2017; Jayasundara et al., 2017). For instance, acclimatisation to cope with environmental stress could shift the community's basal metabolism during the growth phase, thereby reducing the energy available for other stressors. According to the pollution-induced community tolerance concept (Blanck et al., 1988), exposure to stressors usually leads to the selection of the most tolerant species and the disappearance of the most sensitive species, leading to a shift in the community composition that might change the molecular/physiological/functional sensitivity of the entire microbial community. In this context, some of the monthly sensitivity shifts observed in our study may derive from taxonomic fluctuations, leading to variations at the molecular/biochemical level associated with organism susceptibility (Merbt et al., 2022; Liu et al., 2019). Although taxonomic changes do not always influence community functioning owing to functional redundancy, basal metabolism could be modulated by the loss of species, ensuring specialised pathways (Burel et al., 2023; Proia et al., 2011). In the present study, although preliminary, our results showed a clear shift in the algal community in the pond over the time frame, which could contribute to a change in basal metabolism and/or its sensitivity to TBA.

Beyond biological and ecological processes, the variability in the meta-metabolome response to TBA throughout the year may also stem from data analysis strategies. Although the QA/QC procedure confirmed the stability of the analytic systems (mass accuracy, signal intensity, and retention time), variations in the matrix composition (*e.g.* EPS) could cause differences in extraction recoveries and matrix extinction or enhancement at the ESI source level, influencing the meta-metabolome fingerprint independent of biological factors (Gertsman and Barshop, 2018). Additionally, based on the variation in the number of signals per month at each step of the analytical pipeline, the CV indicated information loss during the workflow (Fig. 1). A comparison of CV revealed increased variance between months along the analytical pipeline, suggesting that feature prioritisation associated with TBA exposure may have increased the differences between months by focusing on the modulated part of the dataset. This highlights the challenges in analysing large metabolomics datasets, especially in studies with multiple

sampling times, regarding the reproducibility and repeatability of extraction recovery, chromatographic separation, ionisation efficiency, and data processing (Lennon et al., 2024).

Overall, meta-metabolomics enables investigation of ecotoxicological responses across multiple biological pathways, revealing potential unknown effects of contaminants on microbial communities. In this study, the discrepancies noted in the meta-metabolome response between the months across the period suggest that molecular/biochemical toxicity pathways of TBA may differ.

4.3. Insights on metabolite classes involved in the molecular response to TBA

Beyond the chemical landscape depicted by the TOF data, Q-Exactive datasets provided further insight into distinct versus common metabolite classes associated with TBA exposure. Indeed, among the major contributors that were accurately annotated, the majority differed between the months, confirming the discrepancies noted at the metabolite class level.

Nevertheless, our study revealed putative metabolites associated with TBA concentrations at all months, including oxylipins and other fatty acids (*i.e.* linoleic acid (L2b), 9, 10 DiHODE, 9,12,13-TriHOME, 9,10,12,13-Tetrahydroxyoctadecanoic acid (L3), calostomal (L3), sativic acid (L3), and targeted PG (16.0_18.1)) (Walker et al., 2021; De Carvalho and Caramujo, 2018; Iyer et al., 2015). These metabolites showed heterogeneous trends across the TBA gradient (*e.g.* decrease, increase, and U), suggesting they may not share the same toxicity pathway. In additions to lipids, other responsive classes included amino acids (*i.e.* vicenistatin and Ne-*Ne*-dimethyllysine (L3), S-(2-sulfoethyl)-L-cysteine, deferitrin (L3)), macrolides (*i.e.* 12(*S*)-hydroperoxylsarcoph-10-ene (L3),), mono- and diterpene lactones (*i.e.* 1-deoxybacrispine (L3)) and sesquiterpenoid (*i.e.* 3-{[4-(furan-2-carbonyl)piperazin-1-yl] methyl}-4a-hydroxy-5-methoxy-5,8a-dimethyl-dodeca-hydronaphtho [2,3-*b*]furan-2-one (L3)). In the literature, these metabolites have been linked to various processes such as chemical competition (*i.e.* biotoxin properties and antimicrobial activity), energetic metabolism (*i.e.* carbohydrate catabolism and alternative energetic molecules), and unknown toxicity pathway (Hutchinson et al., 1983; Li and Du, 2022; Oliveira et al., 2011; Liang et al., 2022; Booij et al., 2014).

Furthermore, TBA and other triazine herbicides (*i.e.* atrazine, terbutryn, and prometryn) have been reported to alter mitochondrial energy metabolism. It affects the expression of genes encoding enzymes (*i.e.* citrate synthase and malate synthase) involved in the tricarboxylic acid (TCA) cycle, and reduces mitochondrial respiration in phototrophs (Hawxby et al., 1977; Wang et al., 2022). In addition, by inhibiting photosynthesis, TBA disrupts global energy metabolism related to light energy harvesting, leading to a decrease in energetic molecules (*i.e.* NADH and NADPH). This reduction can lead to energy deficiency, raising questions about the energy costs associated with triazine exposure (Majewska et al., 2021; Wang et al., 2022). Therefore, it can be hypothesized that the uncorrelated putative metabolites found in our study may be part of the defence/response pathway activated to cope with the potential impairment in energy metabolism. The mid- to long-term loss of energetic resources may lead to a taxonomic shift due to starvation or reduced competitiveness (Jayasundara et al., 2017; Tlili et al., 2015).

Altogether, molecular results suggested that TBA may potentially influence lipid metabolism, energy metabolism, and the metabolite classes involved in chemical communication, whether related to defence pathway (*e.g.* alkaloids and terpenoids). This modulation could potentially lead to functional/taxonomic shift in periphyton, which may threaten ecosystem function (Śliwińska-Wilczewska et al., 2021). Because many metabolites remain unidentified, a clear picture of all the toxicity pathways involved could not be established, leaving much of the holistic sensitivity response within a black box. Nevertheless, the identified metabolite classes responsive to TBA could be used as references for future targeted metabolomics approaches.

4.4. Metabolite classes correlated with the photosynthesis inhibition by TBA

Based on the known mode of action of TBA and its associated effects on photosystems (Fiori and Pistocchi, 2014; Rutherford and Krieger-Liszkay, 2001), targeted analyses of photosynthetic pigments and oxylipins were conducted. Contrary to expectations, the targeted pigments (chlorophyll *a*, chlorophyll *c*2, chlorophyll *b*, pheophorbide *a*, fucoxanthin, zeaxanthin, and lutein) showed no significant responses, whereas some annotated oxylipins and lipids decreased with TBA exposure. Notably, hydroxy-octadecaenoic acids (*i.e.* 15(16)-EpODE (L3), 9(10)-EpODE (L3), and 9(*S*)-HPODE (L3)) metabolites of the non-enzymatic oxidation of polyunsaturated fatty acids, were modulated, suggesting a link to oxidative stress (Iyer et al., 2015; Koch et al., 2022; Walker et al., 2021). These results aligned with correlation analysis of untargeted datasets, showing associations between photosynthetic yield fluctuation, some oxylipins (C16-C18) (*i.e.* 9(*S*)-HOTrE (L3), Resolvin E1 (L3), 13-HOTE (L3)) and antioxidants (*i.e.* isolongifolene (L3), Cyclo(L-Leu-L-Arg) (L3); Balakrishnan et al., 2018; Furukawa et al., 2012).

By inhibiting PSII and reducing its light energy-harvesting capacity, TBA triggers the accumulation of oxidative oxygen species (Cañero et al., 2011; Fiori and Pistocchi, 2014) and increases the levels of oxylipins and oxidative stress-related compounds (He and Ding, 2020; Koch et al., 2022). However, this study found that TBA exposure led to a decrease in abundance of metabolites commonly associated with oxidative stress (*e.g.* oxylipins). The identified metabolites were those with significant dose-dependent responses in both the targeted (April 2022) and untargeted annotated compound datasets (with a quadratic trend response). This suggested an acclimatisation mechanism against oxidative stress or TBA's electron chain disrupting effect of TBA (*e.g.* the water-water cycle) (Nguyen and Kim, 2024; Asada, 2006). It would be relevant to investigate the response to TBA of other indicators that are specific to the release of excessive energy harvesting (*i.e.* the xanthophyll cycle) and quenching of oxidative stress (*i.e.* antioxidant enzyme activities) to support this hypothesis (Bonnineau et al., 2013; Latowski et al., 2011).

In addition to compounds usually associated with oxidative stress, several metabolite classes related to the stress response and defence pathway were also correlated with photosynthesis inhibition. Among these classes, alkaloids (*i.e.* vanilloside (L3), Cyclizidine G (L3), Actinopyrone A (L3)) are specialised metabolites involved in response to stress and biotic interactions (Srivastava et al., 2022). Other relevant classes were also found, including terpenoids (*i.e.* cryptoporic acid B (L3)) and peptides (*i.e.* cis-cyclo-(His, Leu) (L3), N(6)-(octanoyl)lysine), which are likely to participate in biofilm communication and stress defence (Kang and Kwak, 2024; Pervaiz et al., 2022; Sarıkahya et al., 2011). These three classes indicated that molecular/biochemical processes, especially alkaloids, undergo photosynthetic inhibition to cope with stress (Matsuura et al., 2014; Yu et al., 2024). Nevertheless, because many metabolites correlated with photosynthetic inhibition remain unidentified, other biochemical toxicity pathways may also be involved. In addition, most of the correlated putative metabolites were specific to a single month, while the physiological response remained relatively similar from one month to another. This suggests that the physiological effects of TBA on photosynthesis may arise from various molecular processes/pathways modulated by the chemical stress, highlighting how the elucidation of ecotoxicity pathways in such a complex community as a whole is a challenging task.

5. Conclusions and perspectives

This study highlights the high variability of the meta-metabolome response and sensitivity (for both whole and annotated datasets)

between several months across a period of one year and a half. These results suggest that the meta-metabolome is more sensitive to chemical stress than photosynthetic yield, reinforcing the value of an aggregated meta-metabolome response to provide an integrative picture of microbial community sensitivity. However, the observed heterogeneity in meta-metabolome sensitivity and response patterns, such as the number of metabolites and trends, points to gaps in our understanding of community molecular and biochemical shifts, which complicates the interpretation of responses under both laboratory and field conditions. This suggests that molecular/biochemical toxicity pathways of TBA may differ from one month to another, as reflected in the variable metabolite trends, classes, and sensitivities observed. Low but significant sensitivity shifts in photosynthesis between months raise questions about the interpretability of molecular/biochemical status in terms of the actual consequences on the physiology and functioning of the community. These findings suggest that similar physiological responses may arise from various molecular pathways, adding complexity to the underlying phenomenon.

In accordance with known TBA's mode of action, correlated metabolites, including oxylipins and pigments, and less-expected putative metabolites belonging to the alkaloid, amino acid, and peptide classes, were described. Additionally, uncorrelated putative metabolites involved in lipid metabolism, energy metabolism, and chemical communication highlight potential new modes of action for TBA. Such modulation might further lead to functional and taxonomic shifts in biofilms after longer exposure.

Further investigation is ongoing to gain knowledge of the environmental drivers of monthly variations in the basal meta-metabolome, the physiological status, their sensitivity and the taxonomic composition in periphyton. Additional experiments with several sampling times incorporating targeted lipids and energetic and oxidative stress endpoints should be implemented to unravel the sequence of events between molecular, structural, and functional responses to TBA towards photosynthesis impairment, leading to potential functional impairment and community shifts in the mid- to long-term (*i.e.* over a month of exposure).

CRediT authorship contribution statement

Arthur Medina: Writing – review & editing, Writing – original draft, Methodology, Investigation, Formal analysis, Data curation, Conceptualization. **Melissa Eon:** Supervision, Methodology, Investigation, Conceptualization. **Nicolas Mazzella:** Writing – review & editing, Supervision, Conceptualization. **Chloé Bonnineau:** Writing – review & editing, Methodology, Data curation. **Débora Millan-Navarro:** Resources. **Aurelie Moreira:** Supervision, Software, Resources. **Soizic Morin:** Writing – review & editing, Validation, Project administration, Funding acquisition. **Nicolas Creusot:** Writing – review & editing, Writing – original draft, Visualization, Validation, Supervision, Software, Resources, Project administration, Methodology, Investigation, Funding acquisition, Formal analysis, Data curation, Conceptualization.

Declaration of competing interest

The authors declare that they have no known competing financial interests or personal relationships that could have appeared to influence the work reported in this paper.

Acknowledgements

This study was funded by the INRAE and MICROBIOMIQ projects (INRAE metaprogram BIOSEFAIR). This work was carried out with the support (equipment and staff) provided by the XPO scientific infrastructure (DOI:10.17180/brey-mr38, part of the LIFE research infrastructure–Living in Freshwater and Estuaries, INRAE) of the EABX research unit and by the Bordeaux Metabolome facility as a member of the French infrastructure of metabolomics and fluxomics (MetaboHUB, ANR). The authors thank J. Valls Fonayet for providing support and collaboration regarding the use of the UHPLC-Q-Exactive+ mass spectrometer (UMR1366 Oenologie).

Appendix A. Supplementary data

Supplementary data to this article can be found online at https://doi.org/10.1016/j.scitotenv.2024.177681.

Data availability

Data will be made available on request.

References

Asada, K., 2006. Production and scavenging of reactive oxygen species in chloroplasts and their functions. Plant Physiol. 141, 391–396. https://doi.org/10.1104/pp.106.082040.

Balakrishnan, R., Elangovan, N., Mohankumar, T., Nataraj, J., Manivasagam, T., Justin Thenmozhi, A., Essa, M.M., Akbar, M., Abdul Sattar Khan, M., 2018. Isolongifolene attenuates rotenone-induced mitochondrial dysfunction, oxidative stress and apoptosis. Front. Biosci. (Schol. Ed.) 10, 248–261. https://doi.org/10.2741/s513.

Battaglino, B., Grinzato, A., Pagliano, C., 2021. Binding properties of photosynthetic herbicides with the QB site of the D1 protein in plant photosystem II: a combined functional and molecular docking study. Plants (Basel) 10, 1501. https://doi.org/10.3390/plants10081501.

Battin, T.J., Besemer, K., Bengtsson, M.M., Romani, A.M., Packmann, A.I., 2016. The ecology and biogeochemistry of stream biofilms. Nat. Rev. Microbiol. 14, 251–263. https://doi.org/10.1038/nrmicro.2016.15.

Becker, R.A., Chambers, J.M., Wilks, A.R., 1988. The New S Language: A Programming Environment for Data Analysis and Graphics, Wadsworth & Brooks/Cole Computer Science Series. Wadsworth & Brooks/Cole Advanced Books & Software, Pacific Grove, Calif.

Bedia, C., 2022. Metabolomics in environmental toxicology: applications and challenges. Trends in Environmental Analytical Chemistry 34, e00161. https://doi.org/10.1016/j.teac.2022.e00161.

Beketov, M.A., Kefford, B.J., Schäfer, R.B., Liess, M., 2013. Pesticides reduce regional biodiversity of stream invertebrates. Proc. Natl. Acad. Sci. U. S. A. 110, 11039–11043. https://doi.org/10.1073/pnas.1305618110.

Beronius, A., Zilliacus, J., Hanberg, A., Luijten, M., van der Voet, H., van Klaveren, J., 2020. Methodology for health risk assessment of combined exposures to multiple chemicals. Food Chem. Toxicol. 143, 111520. https://doi.org/10.1016/j.fct.2020.111520.

Blanck, H., Wängberg, S.-Å., Molander, S., 1988. Pollution-induced Community Tolerance—A New Ecotoxicological Tool. https://doi.org/10.1520/STP26265S.

Booij, P., Lamoree, M.H., Sjollema, S.B., Voogt, P.de, Schollee, J.E., Vethaak, A.D., Leonards, P.E.G., 2014. Non-target Metabolomic Profiling of the Marine Microalgae Dunaliella tertiolecta After Exposure to Diuron using Complementary High-Resolution Analytical Techniques. Curr. Metabolomics 2, 213–222. https://doi.org/10.2174/2213235X02666140922222901.

Bonnineau, C., Tlili, A., Faggiano, L., Montuelle, B., Guasch, H., 2013. The use of antioxidant enzymes in freshwater biofilms: temporal variability vs. toxicological responses. Aquat. Toxicol. 136–137, 60–71. https://doi.org/10.1016/j.aquatox.2013.03.009.

Bonnineau, C., Artigas, J., Chaumet, B., Dabrin, A., Faburé, J., Ferrari, B.J.D., Lebrun, J. D., Margoum, C., Mazzella, N., Miège, C., Morin, S., Uher, E., Babut, M., Pesce, S., 2020. Role of biofilms in contaminant bioaccumulation and trophic transfer in aquatic ecosystems: current state of knowledge and future challenges. In: de Voogt, P. (Ed.), Reviews of Environmental Contamination and Toxicology Volume 253, Reviews of Environmental Contamination and Toxicology. Springer International Publishing, Cham, pp. 115–153. https://doi.org/10.1007/398_2019_39.

Burel, M., Régimbeau, A., Chaffron, S., Eveillard, D., Pelletier, E., 2023. PhotoEukStein: Towards an Omics-based Definition of Unicellular Eukaryote Phototrophs Functional Traits Via Metabolic Modelling. https://doi.org/10.1101/2023.05.22.541783.

Cañero, A.I., Cox, L., Redondo-Gómez, S., Mateos-Naranjo, E., Hermosín, M.C., Cornejo, J., 2011. Effect of the herbicides terbuthylazine and glyphosate on photosystem II photochemistry of young olive (Olea europaea) plants. J. Agric. Food Chem. 59, 5528–5534. https://doi.org/10.1021/jf200875u.

Chaumet, B., Mazzella, N., Neury-Ormanni, J., Morin, S., 2020. Light and temperature influence on diuron bioaccumulation and toxicity in biofilms. Ecotoxicology 29, 185–195. https://doi.org/10.1007/s10646-020-02166-8.

Colas, S., Marie, B., Morin, S., Milhe-Poutingon, M., Foucault, P., Chalvin, S., Gelber, C., Baldoni-Andrey, P., Gurieff, N., Fortin, C., Faucheur, S.L., 2023. New Sensitive Tools to Characterize Meta-metabolome Response to Short- and Long-term Cobalt Exposure in Dynamic River Biofilm Communities. https://doi.org/10.1101/2023.11.16.567369.

Colas, S., Marie, B., Milhe-Poutingon, M., Lot, M.-C., Boullemant, A., Fortin, C., Le Faucheur, S., 2024. Meta-metabolomic responses of river biofilms to cobalt exposure

and use of dose-response model trends as an indicator of effects. J. Hazard. Mater. 470, 134099. https://doi.org/10.1016/j.jhazmat.2024.134099.
Corcoll, N., Ricart, M., Franz, S., Sans-Piché, F., Schmitt-Jansen, M., Guasch, H., 2012. The use of photosynthetic fluorescence parameters from autotrophic biofilms for monitoring the effect of chemicals in river ecosystems. In: Guasch, H., Ginebreda, A., Geiszinger, A. (Eds.), Emerging and Priority Pollutants in Rivers: Bringing Science into River Management Plans. The Handbook of Environmental Chemistry. Springer, Berlin, Heidelberg, pp. 85–115. https://doi.org/10.1007/978-3-642-25722-3_4.
Creusot, N., Chaumet, B., Eon, M., Mazzella, N., Moreira, A., Morin, S., 2022. Metabolomics insight into the influence of environmental factors in responses of freshwater biofilms to the model herbicide diuron. Environ. Sci. Pollut. Res. 29, 29332–29347. https://doi.org/10.1007/s11356-021-17072-7.
De Carvalho, C.C.C.R., Caramujo, M.J., 2018. The various roles of fatty acids. Molecules 23, 2583. https://doi.org/10.3390/molecules23102583.
Delignette-Muller, M.L., Siberchicot, A., Larras, F., Billoir, E., 2023. DRomics, a Workflow to Model and Make Sense of Dose-response (Multi-)omics Data in (Eco) Toxicology. https://doi.org/10.1101/2023.02.09.527852.
Dias, D.A., Jones, O.A.H., Beale, D.J., Boughton, B.A., Benheim, D., Kouremenos, K.A., Wolfender, J.-L., Wishart, D.S., 2016. Current and future perspectives on the structural identification of small molecules in biological systems. Metabolites 6, 46. https://doi.org/10.3390/metabo6040046.
Djoumbou Feunang, Y., Eisner, R., Knox, C., Chepelev, L., Hastings, J., Owen, G., Fahy, E., Steinbeck, C., Subramanian, S., Bolton, E., Greiner, R., Wishart, D.S., 2016. ClassyFire: automated chemical classification with a comprehensive, computable taxonomy. J. Chem. 8, 61. https://doi.org/10.1186/s13321-016-0174-y.
Dührkop, K., Fleischauer, M., Ludwig, M., Aksenov, A.A., Melnik, A.V., Meusel, M., Dorrestein, P.C., Rousu, J., Böcker, S., 2019. SIRIUS 4: a rapid tool for turning tandem mass spectra into metabolite structure information. Nat. Methods 16, 299–302. https://doi.org/10.1038/s41592-019-0344-8.
EFSA Scientific Committee, Susan Barlow, Andrew Chesson, John D. Collins, Albert Flynn, Anthony Hardy, Klaus-Dieter Jany, Ada Knaap, Harry Kuiper, John-Christian Larsen, David Lovell, Pierre Le Neindre, Jan Schans, Josef Schlatter, Vittorio Silano, Staffan Skerfving, Philippe Vannier, 2009. Guidance of the Scientific Committee on Use of the Benchmark Dose Approach in Risk Assessment. EFS2 7. doi:https://doi.org/10.2903/j.efsa.2009.1150.
EFSA Scientific Committee, E.F.S., Hardy, A., Benford, D., Halldorsson, T., Jeger, M.J., Knutsen, K.H., More, S., Mortensen, A., Naegeli, H., Noteborn, H., Ockleford, C., Ricci, A., Rychen, G., Silano, V., Solecki, R., Turck, D., Aerts, M., Bodin, L., Davis, A., Edler, L., Gundert-Remy, U., Sand, S., Slob, W., Bottex, B., Abrahantes, J.C., Marques, D.C., Kass, G., Schlatter, J.R., 2017. Update: use of the benchmark dose approach in risk assessment. EFSA J. 15, e04658. doi:https://doi.org/10.2903/j.efsa.2017.4658.
Eymery, F., Botta, F., Farama, E., Rety, J., Tessier, N., Yamada, O., Bedos, C., Blanchoud, H., Camel, V., Caudeville, J., Cotelle, S., Dauchy, X., Lavison-Bompard, G., Millet, M., Nicolai, M., 2021. Occurrence de la terbuthylazine dans les eaux de surface - Signalements n° 57 et 59 (Report) (Anses).
Finizio, A., Grenni, P., Petrangeli, A.B., Barra Caracciolo, A., Santoro, S., Di Guardo, A., 2022. Use of large datasets of measured environmental concentrations for the ecological risk assessment of chemical mixtures in Italian streams: a case study. Sci. Total Environ. 806, 150614. https://doi.org/10.1016/j.scitotenv.2021.150614.
Fiori, E., Pistocchi, R., 2014. Skeletonema marinoi (Bacillariophyceae) sensitivity to herbicides and effects of temperature increase on cellular responses to terbuthylazine exposure. Aquat. Toxicol. 147, 112–120. https://doi.org/10.1016/j.aquatox.2013.12.014.
Fraisier-Vannier, O., Chervin, J., Cabanac, G., Puech, V., Fournier, S., Durand, V., Amiel, A., André, O., Benamar, O.A., Dumas, B., Tsugawa, H., Marti, G., 2020. MS-CleanR: a feature-filtering workflow for untargeted LC–MS based metabolomics. Anal. Chem. 92, 9971–9981. https://doi.org/10.1021/acs.analchem.0c01594.
Furukawa, T., Akutagawa, T., Funatani, H., Uchida, T., Hotta, Y., Niwa, M., Takaya, Y., 2012. Cyclic dipeptides exhibit potency for scavenging radicals. Bioorganic & Medicinal Chemistry, The Chemistry Biology Interface 20, 2002–2009. https://doi.org/10.1016/j.bmc.2012.01.050.
Garrido, E., Díaz, M.F., Bernal, H., Ñustez, C.E., Thaler, J., Jander, G., Poveda, K., 2017. Costs and tradeoffs of resistance and tolerance to belowground herbivory in potato. PloS One 12, e0169083. https://doi.org/10.1371/journal.pone.0169083.
Gauthier, L., Tison-Rosebery, J., Morin, S., Mazzella, N., 2020. Metabolome response to anthropogenic contamination on microalgae: a review. Metabolomics 16, 8. https://doi.org/10.1007/s11306-019-1628-9.
Gertsman, I., Barshop, B.A., 2018. Promises and pitfalls of untargeted metabolomics. J. Inherit. Metab. Dis. 41, 355–366. https://doi.org/10.1007/s10545-017-0130-7.
Giacomoni, F., Le Corguillé, G., Monsoor, M., Landi, M., Pericard, P., Pétéra, M., Duperier, C., Tremblay-Franco, M., Martin, J.-F., Jacob, D., Goulitquer, S., Thévenot, E.A., Caron, C., 2014. Workflow4Metabolomics: a collaborative research infrastructure for computational metabolomics. Bioinformatics 31, 1493–1495. https://doi.org/10.1093/bioinformatics/btu813.
Gil Solsona, R., Alvarez-Muñoz, D., Serra-Compte, A., Rodríguez-Mozaz, S., 2021. (Xeno) metabolomics for the evaluation of aquatic organism's exposure to field contaminated water. Trends in Environmental Analytical Chemistry 31, e00132. https://doi.org/10.1016/j.teac.2021.e00132.
Gomes, M.P., Juneau, P., 2017. Temperature and light modulation of herbicide toxicity on algal and cyanobacterial physiology. Front. Environ. Sci. 5, 50. https://doi.org/10.3389/fenvs.2017.00050.
Guasch, H., Artigas, J., Bonet, B., Bonnineau, C., Canals, O., Corcoll, N., Foulquier, A., López-Doval, J., Kim-Tiam, S., Morin, S., Navarro, E., Pesce, S., Proia, L., Salvadó, H., Serra, A., 2016. The use of biofilms to assess the effects of chemicals on freshwater ecosystems. In: Aquatic Biofilms: Ecology, Water Quality and Wastewater Treatment. Caister Academic Press, pp. 125–144. https://doi.org/10.21775/9781910190173.07.
Hawxby, K., Tubea, B., Ownby, J., Basler, E., 1977. Effects of various classes of herbicides on four species of algae. Pestic. Biochem. Physiol. 7, 203–209. https://doi.org/10.1016/0048-3575(77)90011-6.
He, M., Ding, N.-Z., 2020. Plant unsaturated fatty acids: multiple roles in stress response. Frontiers in Plant Sci. 11.
Henderson, C.M., Shulman, N.J., MacLean, B., MacCoss, M.J., Hoofnagle, A.N., 2018. Skyline performs as well as vendor software in the quantitative analysis of serum 25-Hydroxy vitamin D and vitamin D binding globulin. Clin. Chem. 64, 408–410. https://doi.org/10.1373/clinchem.2017.282293.
Herlory, O., 2005. Etude du biofilm microalgal des vasieres intertidales: dynamique spatio-temporelle a micro-echelle et performances photosynthetiques, p. 240.
Hutchinson, C.R., Shu-Wen, L., McInnes, A.G., Walter, J.A., 1983. Comparative biochemistry of fatty acid and macrolide antibiotic (brefeldin a). Formation in *penicillium brefeldianum*. Tetrahedron 39, 3507–3513. https://doi.org/10.1016/S0040-4020(01)88660-9.
Iyer, E.S.S., Gdor, I., Eliash, T., Sheves, M., Ruhman, S., 2015. Efficient femtosecond energy transfer from carotenoid to retinal in gloeobacter rhodopsin–salinixanthin complex. J. Phys. Chem. B 119, 2345–2349. https://doi.org/10.1021/jp506639w.
Jayasundara, N., Fernando, P.W., Osterberg, J.S., Cammen, K.M., Schultz, T.F., Di Giulio, R.T., 2017. Cost of tolerance: physiological consequences of evolved resistance to inhabit a polluted environment in teleost fish Fundulus heteroclitus. Environ. Sci. Technol. 51, 8763–8772. https://doi.org/10.1021/acs.est.7b01913.
Kang, S.-O., Kwak, M.-K., 2024. Antimicrobial cyclic dipeptides from Japanese quail (Coturnix japonica) eggs supplemented with probiotic lactobacillus plantarum. J. Microbiol. Biotechnol. 34, 314–329. https://doi.org/10.4014/jmb.2311.11006.
Kim, H.W., Wang, M., Leber, C., Nothias, L.-F., Reher, R., Kang, K.B., Hooft, J.J.J., Dorrestein, P., Gerwick, W., Cottrell, G., 2021. NPClassifier: a deep neural network-based structural classification tool for natural products. J. Nat. Prod. 84. https://doi.org/10.1021/acs.jnatprod.1c00399.
Koch, E., Wiebel, M., Löwen, A., Willenberg, I., Schebb, N.H., 2022. Characterization of the oxylipin pattern and other fatty acid oxidation products in freshly pressed and stored plant oils. J. Agric. Food Chem. 70, 12935–12945. https://doi.org/10.1021/acs.jafc.2c04987.
Larras, F., Billoir, E., Baillard, V., Siberchicot, A., Scholz, S., Wubet, T., Tarkka, M., Schmitt-Jansen, M., Delignette-Muller, M.-L., 2018. DRomics: a turnkey tool to support the use of the dose–response framework for omics data in ecological risk assessment. Environ. Sci. Technol. 52, 14461–14468. https://doi.org/10.1021/acs.est.8b04752.
Larras, F., Billoir, E., Scholz, S., Tarkka, M., Wubet, T., Delignette-Muller, M.-L., Schmitt-Jansen, M., 2020. A multi-omics concentration-response framework uncovers novel understanding of triclosan effects in the chlorophyte Scenedesmus vacuolatus. J. Hazard. Mater. 397, 122727. https://doi.org/10.1016/j.jhazmat.2020.122727.
Latowski, D., Kuczyńska, P., Strzałka, K., 2011. Xanthophyll cycle—a mechanism protecting plants against oxidative stress. Redox Rep. 16, 78–90. https://doi.org/10.1179/174329211X13020951739938.
Lee, H.-J., Kremer, D.M., Sajjakulnukit, P., Zhang, L., Lyssiotis, C.A., 2019. A large-scale analysis of targeted metabolomics data from heterogeneous biological samples provides insights into metabolite dynamics. Metabolomics 15, 103. https://doi.org/10.1007/s11306-019-1564-8.
Lennon, S., Chaker, J., Price, E.J., Hollender, J., Huber, C., Schulze, T., Ahrens, L., Béen, F., Creusot, N., Debrauwer, L., Dervilly, G., Gabriel, C., Guérin, T., Habchi, B., Jamin, E.L., Klánová, J., Kosjek, T., Le Bizec, B., Meijer, J., Mol, H., Nijssen, R., Oberacher, H., Papaioannou, N., Parinet, J., Sarigiannis, D., Stravs, M.A., Tkalec, Ž., Schymanski, E.L., Lamoree, M., Antignac, J.-P., David, A., 2024. Harmonized quality assurance/quality control provisions to assess completeness and robustness of MS1 data preprocessing for LC-HRMS-based suspect screening and non-targeted analysis. TrAC Trends Anal. Chem. 174, 117674. https://doi.org/10.1016/j.trac.2024.117674.
Li, N., Du, Q., 2022. A new source of diterpene lactones from Andrographis paniculata (Burm. f.) nees—two endophytic fungi of Colletotrichum sp. with antibacterial and antioxidant activities. Front. Microbiol. 13. https://doi.org/10.3389/fmicb.2022.819770.
Li, Z., Lu, Y., Guo, Y., Cao, H., Wang, Q., Shui, W., 2018. Comprehensive evaluation of untargeted metabolomics data processing software in feature detection, quantification and discriminating marker selection. Anal. Chim. Acta 1029, 50–57. https://doi.org/10.1016/j.aca.2018.05.001.
Liang, Z., Li, J., Ling, C., Xu, R., Yi, X., Ju, J., Li, Q., 2022. Characterization of the Aminosugar Biosynthetic and Regulatory Genes of Vicenistatin in Monodonata labio-Associated Streptomyces parvus SCSIO Mla-L010. J. Nat. Prod. 85, 256–263. https://doi.org/10.1021/acs.jnatprod.1c01044.
Lips, S., Larras, F., Schmitt-Jansen, M., 2022. Community metabolomics provides insights into mechanisms of pollution-induced community tolerance of periphyton. Sci. Total Environ. 824, 153777. https://doi.org/10.1016/j.scitotenv.2022.153777.
Liu, J., Meng, Z., Liu, X., Zhang, X.-H., 2019. Microbial assembly, interaction, functioning, activity and diversification: a review derived from community compositional data. Mar Life Sci Technol 1, 112–128. https://doi.org/10.1007/s42995-019-00004-3.
MacLean, B., Tomazela, D.M., Shulman, N., Chambers, M., Finney, G.L., Frewen, B., Kern, R., Tabb, D.L., Liebler, D.C., MacCoss, M.J., 2010. Skyline: an open source document editor for creating and analyzing targeted proteomics experiments. Bioinformatics 26, 966–968. https://doi.org/10.1093/bioinformatics/btq054.
Majewska, M., Harshkova, D., Pokora, W., Baścik-Remisiewicz, A., Tułodziecki, S., Aksmann, A., 2021. Does diclofenac act like a photosynthetic herbicide on green algae? *Chlamydomonas reinhardtii* synchronous culture-based study with atrazine as

reference. Ecotoxicol. Environ. Saf. 208, 111630. https://doi.org/10.1016/j.ecoenv.2020.111630.
Margoum, C., Rocco, K., Aprianto, Y., Artigas, J., Benoit, P., Chaumot, A., Coquery, M., Creusot, N., Delorme, N., Devaux, J., Eon, M., Gouy-Boussada, V., Guillemain, C., Heinisch, S., Jan, G., Mamy, L., Millan-Navarro, D., Richard, L., Sand, C., Morin, S., Veron, J., Viemont-Lefeuvre, I., Bonnineau, C., 2023. Identification et écotoxicité des produits de transformation des pesticides dans les milieux aquatiques. In: 51ème Congrès Du Groupe Français de Recherches Sur Les Pesticides. Paris, France.
Matsuura, H.N., Rau, M.R., Fett-Neto, A.G., 2014. Oxidative stress and production of bioactive monoterpene indole alkaloids: biotechnological implications. Biotechnol. Lett. 36, 191–200. https://doi.org/10.1007/s10529-013-1348-6.
Mazzella, N., Moreira, Aurélie, Eon, Melissa, Médina, Arthur, Millan-Navarro, Débora, Creusot, Nicolas, 2023. Hydrophilic interaction liquid chromatography coupled with tandem mass spectrometry method for quantification of five phospholipid classes in various matrices. MethodsX 10, 102026. https://doi.org/10.1016/j.mex.2023.102026.
Merbt, S.N., Kroll, A., Tamminen, M., Rühs, P.A., Wagner, B., Sgier, L., Sembalova, O., Abel, B., Tlili, A., Schirmer, K., Behra, R., 2022. Influence of microplastics on microbial structure, function, and mechanical properties of stream periphyton. Front. Environ. Sci. 10. https://doi.org/10.3389/fenvs.2022.928247.
Morin, S., Artigas, J., 2023. Twenty years of research in ecosystem functions in aquatic microbial ecotoxicology. Environ. Toxicol. Chem. 42, 1867–1888. https://doi.org/10.1002/etc.5708.
Morin, S., Chaumet, B., Mazzella, N., 2018. A time-dose response model to assess Diuron-induced photosynthesis inhibition in freshwater biofilms. Front. Environ. Sci. 6, 131. https://doi.org/10.3389/fenvs.2018.00131.
Neury-Ormanni, J., 2021. Impact de la saisonnalité et d'une contamination pesticide environnementale sur des relations biotiques entre la micro-méiofaune et les microalgues d'un biofilm d'eau douce, p. 209.
Nguyen, M.K., Kim, H.M., 2024. A review of the representative microalgal-derived reactive oxygen species: possible formation, ecophysiological implications, and metabolomic-based evaluations. J. Appl. Phycol. 36, 129–154. https://doi.org/10.1007/s10811-023-03132-7.
Nyamundanda, G., Brennan, L., Gormley, I.C., 2010. Probabilistic principal component analysis for metabolomic data. BMC Bioinformatics 11, 571. https://doi.org/10.1186/1471-2105-11-571.
Oliveira, C.M. de, Silva, G.H., Regasini, L.O., Flausino, O.Jr., López, S.N., Abissi, B.M., Berlinck, R.G. de S., Sette, L.D., Bonugli-Santos, R.C., Rodrigues, A., Bolzani, V. da S., Araujo, A.R., 2011. Xylarenones C−E from an endophytic fungus isolated from Alibertia macrophylla. J. Nat. Prod. 74, 1353–1357. doi:https://doi.org/10.1021/np1005983.
Pervaiz, I., Hasnat, M., Ahmad, S., Khurshid, U., Saleem, H., Alshammari, F., Almansour, K., Mollica, A., Rengasamy, K.R.R., Zainal Abidin, S.A., Anwar, S., 2022. Phytochemical composition, biological propensities, and *in-silico* studies of *Crateva adansonii DC.*: a natural source of bioactive compounds. Food Bioscience 49, 101890. https://doi.org/10.1016/j.fbio.2022.101890.
Pesce, S., Perceval, O., Bonnineau, C., Casado-Martinez, C., Dabrin, A., Lyautey, E., Naffrechoux, E., Ferrari, B.J.D., 2018. Looking at biological community level to improve ecotoxicological assessment of freshwater sediments: report on a first French-Swiss workshop. Environ. Sci. Pollut. Res. 25, 970–974. https://doi.org/10.1007/s11356-017-0620-z.
Polst, B.H., Allen, J., Hölker, F., Hilt, S., Stibor, H., Gross, E.M., Schmitt-Jansen, M., 2023. Exposure pathways matter: aquatic phototrophic communities respond differently to agricultural run-off exposed via sediment or water. J. Appl. Ecol. 60, 1868–1880. https://doi.org/10.1111/1365-2664.14478.
Proia, L., Morin, S., Peipoch, M., Romaní, A.M., Sabater, S., 2011. Resistance and recovery of river biofilms receiving short pulses of Triclosan and Diuron. Sci. Total Environ. 409, 3129–3137. https://doi.org/10.1016/j.scitotenv.2011.05.013.
Proia, L., Osorio, V., Soley, S., Köck-Schulmeyer, M., Pérez, S., Barceló, D., Romaní, A.M., Sabater, S., 2013. Effects of pesticides and pharmaceuticals on biofilms in a highly impacted river. Environ. Pollut. 178, 220–228. https://doi.org/10.1016/j.envpol.2013.02.022.
Rodríguez-Mozaz, S., Serra-Compte, A., Gil Solsona, R., Alvarez-Muñoz, D., 2020. Environmental Metabolomics and Xenometabolomics for the Assessment of Exposure to Contaminant Mixtures, p. 283. https://doi.org/10.1016/b978-0-12-818196-6.00010-8.
Rožman, M., Lekunberri, I., Grgić, I., Borrego, C.M., Petrović, M., 2023. Effects of combining flow intermittency and exposure to emerging contaminants on the composition and metabolic response of streambed biofilm bacterial communities. Sci. Total Environ. 877, 162818. https://doi.org/10.1016/j.scitotenv.2023.162818.
Rutherford, A.W., Krieger-Liszkay, A., 2001. Herbicide-induced oxidative stress in photosystem II. Trends Biochem. Sci. 26, 648–653. https://doi.org/10.1016/S0968-0004(01)01953-3.
Sabater, S., Timoner, X., Borrego, C., Acuña, V., 2016. Stream biofilm responses to flow intermittency: from cells to ecosystems. Front. Environ. Sci. 4. https://doi.org/10.3389/fenvs.2016.00014.
Sarıkahya, N.B., Pekmez, M., Arda, N., Kayce, P., Yavaşoğlu, N.Ü.K., Kırmızıgül, S., 2011. Isolation and characterization of biologically active glycosides from endemic *Cephalaria* species in Anatolia. Phytochemistry Letters, Special Issue in Honour of Professor Ayhan Ulubelen 4, 415–420. https://doi.org/10.1016/j.phytol.2011.05.006.
Schmitt-Jansen, M., Altenburger, R., 2005. Predicting and observing responses of algal communities to photosystem ii–herbicide exposure using pollution-induced community tolerance and species-sensitivity distributions. Environ. Toxicol. Chem. 24, 304. https://doi.org/10.1897/03-647.1.
Schreiner, V.C., Szöcs, E., Bhowmik, A.K., Vijver, M.G., Schäfer, R.B., 2016. Pesticide mixtures in streams of several European countries and the USA. Sci. Total Environ. 573, 680–689. https://doi.org/10.1016/j.scitotenv.2016.08.163.
Schymanski, E.L., Jeon, J., Gulde, R., Fenner, K., Ruff, M., Singer, H.P., Hollender, J., 2014. Identifying small molecules via high resolution mass spectrometry: communicating confidence. Environ. Sci. Technol. 48, 2097–2098. https://doi.org/10.1021/es5002105.
Serra-Compte, A., Corcoll, N., Huerta, B., Rodríguez-Mozaz, S., Sabater, S., Barceló, D., Álvarez-Muñoz, D., 2018. Fluvial biofilms exposed to desiccation and pharmaceutical pollution: new insights using metabolomics. Sci. Total Environ. 618, 1382–1388. https://doi.org/10.1016/j.scitotenv.2017.09.258.
Śliwińska-Wilczewska, S., Wiśniewska, K., Konarzewska, Z., Cieszyńska, A., Barreiro Felpeto, A., Lewandowska, A.U., Latała, A., 2021. The current state of knowledge on taxonomy, modulating factors, ecological roles, and mode of action of phytoplankton allelochemicals. Sci. Total Environ. 773, 145681. https://doi.org/10.1016/j.scitotenv.2021.145681.
Smedbol, É., Gomes, M.P., Paquet, S., Labrecque, M., Lepage, L., Lucotte, M., Juneau, P., 2018. Effects of low concentrations of glyphosate-based herbicide factor 540® on an agricultural stream freshwater phytoplankton community. Chemosphere 192, 133–141. https://doi.org/10.1016/j.chemosphere.2017.10.128.
Srivastava, R., Prajapati, R., Kanda, T., Yadav, Sadhana, Singh, N., Yadav, Shivam, Mishra, R., Atri, N., 2022. Phycochemistry and bioactivity of cyanobacterial secondary metabolites. Mol. Biol. Rep. 49, 11149–11167. https://doi.org/10.1007/s11033-022-07911-2.
Tasca, A.L., Puccini, M., Fletcher, A., 2018. Terbuthylazine and desethylterbuthylazine: recent occurrence, mobility and removal techniques. Chemosphere 202, 94–104. https://doi.org/10.1016/j.chemosphere.2018.03.091.
Tien, C.-J., Lin, M.-C., Chiu, W.-H., Chen, C.S., 2013. Biodegradation of carbamate pesticides by natural river biofilms in different seasons and their effects on biofilm community structure. Environ. Pollut. 179, 95–104. https://doi.org/10.1016/j.envpol.2013.04.009.
Tison-Rosebery, J., Moreira, S., Eon, M., Campillo, L., Maubert, S., Malepeyre, C., Célerier, J., Sol, V., Vedrenne, J., Bertrin, V., Creusot, N., 2023. Effects of Lagarosiphon major extracts on the metabolome and photosynthesis of Microcystis aeruginosa. C. R. Chim. 26, 1–15. https://doi.org/10.5802/crchim.250.
Tlili, A., Dorigo, U., Montuelle, B., Margoum, C., Carluer, N., Gouy, V., Bouchez, A., Bérard, A., 2008. Responses of chronically contaminated biofilms to short pulses of diuron: an experimental study simulating flooding events in a small river. Aquat. Toxicol. 87, 252–263. https://doi.org/10.1016/j.aquatox.2008.02.004.
Tlili, A., Bérard, A., Roulier, J.-L., Volat, B., Montuelle, B., 2010. PO43− dependence of the tolerance of autotrophic and heterotrophic biofilm communities to copper and diuron. Aquat. Toxicol. 98, 165–177. https://doi.org/10.1016/j.aquatox.2010.02.008.
Tlili, A., Berard, A., Blanck, H., Bouchez, A., 2015. Pollution-induced community tolerance (PICT): towards an ecologically relevant risk assessment of chemicals in aquatic systems. Freshw. Biol. 11.
Toubiana, D., Maruenda, H., 2021. Guidelines for correlation coefficient threshold settings in metabolite correlation networks exemplified on a potato association panel. BMC Bioinformatics 22, 116. https://doi.org/10.1186/s12859-021-03994-z.
Tsugawa, H., Cajka, T., Kind, T., Ma, Y., Higgins, B., Ikeda, K., Kanazawa, M., VanderGheynst, J., Fiehn, O., Arita, M., 2015. MS-DIAL: data-independent MS/MS deconvolution for comprehensive metabolome analysis. Nat. Methods 12, 523–526. https://doi.org/10.1038/nmeth.3393.
Tsugawa, H., Kind, T., Nakabayashi, R., Yukihira, D., Tanaka, W., Cajka, T., Saito, K., Fiehn, O., Arita, M., 2016. Hydrogen rearrangement rules: computational MS/MS fragmentation and structure elucidation using MS-FINDER software. Anal. Chem. 88, 7946–7958. https://doi.org/10.1021/acs.analchem.6b00770.
Vonk, J.A., Kraak, M.H.S., 2020. Herbicide exposure and toxicity to aquatic primary producers. In: de Voogt, P. (Ed.), Reviews of Environmental Contamination and Toxicology Volume 250, Reviews of Environmental Contamination and Toxicology. Springer International Publishing, Cham, pp. 119–171. https://doi.org/10.1007/398_2020_48.
Walker, R.E., Savinova, O.V., Pedersen, T.L., Newman, J.W., Shearer, G.C., 2021. Effects of inflammation and soluble epoxide hydrolase inhibition on oxylipin composition of very low-density lipoproteins in isolated perfused rat livers. Physiol. Rep. 9, e14480. https://doi.org/10.14814/phy2.14480.
Wang, Z., Sun, X., Ru, S., Wang, J., Xiong, J., Yang, L., Hao, L., Zhang, J., Zhang, X., 2022. Effects of co-exposure of the triazine herbicides atrazine, prometryn and terbutryn on *Phaeodactylum tricornutum* photosynthesis and nutritional value. Sci. Total Environ. 807, 150609. https://doi.org/10.1016/j.scitotenv.2021.150609.
Watnick, P., Kolter, R., 2000. Biofilm, city of microbes. J. Bacteriol. 182, 2675–2679. https://doi.org/10.1128/jb.182.10.2675-2679.2000.
Xia, J., Psychogios, N., Young, N., Wishart, D.S., 2009. MetaboAnalyst: a web server for metabolomic data analysis and interpretation. Nucleic Acids Res. 37, W652–W660. https://doi.org/10.1093/nar/gkp356.
Yu, H., Li, D., Wu, Y., Miao, P., Zhou, C., Cheng, H., Dong, Q., Zhao, Y., Liu, Z., Zhou, L., Pan, C., 2024. Integrative omics analyses of tea (*Camellia sinensis*) under glufosinate stress reveal defense mechanisms: a trade-off with flavor loss. J. Hazard. Mater. 473, 134542. https://doi.org/10.1016/j.jhazmat.2024.134542.